J Sci Comput (2018) 76:1938–1967
https://doi.org/10.1007/s10915-018-0690-1

A Uniquely Solvable, Energy Stable Numerical Scheme for the Functionalized Cahn–Hilliard Equation and Its Convergence Analysis

Wenqiang Feng[1] · Zhen Guan[2] · John Lowengrub[2] · Cheng Wang[3] · Steven M. Wise[1] · Ying Chen[4]

Received: 28 March 2017 / Revised: 8 February 2018 / Accepted: 1 March 2018 /
Published online: 6 March 2018

Abstract We present and analyze a uniquely solvable and unconditionally energy stable numerical scheme for the Functionalized Cahn–Hilliard equation, including an analysis of convergence. One key difficulty associated with the energy stability is based on the fact that one nonlinear energy functional term in the expansion is neither convex nor concave. To overcome this subtle difficulty, we add two auxiliary terms to make the combined term convex, which in turns yields a convex–concave decomposition of the physical energy. As a result, both the unconditional unique solvability and the unconditional energy stability of the proposed numerical scheme are assured. In addition, a global in time H^2_{per} stability of the numerical scheme is established at a theoretical level, which in turn ensures the full order convergence analysis of the scheme, which is the first such result in this field. To deal with an implicit 4-Laplacian term at each time step, we apply an efficient preconditioned steepest descent algorithm to solve the corresponding nonlinear systems in the finite difference set-

✉ Cheng Wang
cwang1@umassd.edu

Wenqiang Feng
wfeng1@vols.utk.edu

Zhen Guan
guanz2@math.uci.edu

John Lowengrub
lowengrb@math.uci.edu

Steven M. Wise
swise1@utk.edu

Ying Chen
yingc@math.duke.edu

1 Department of Mathematics, The University of Tennessee, Knoxville, TN 37996, USA

2 Department of Mathematics, The University of California, Irvine, CA 92697, USA

3 Department of Mathematics, The University of Massachusetts, North Dartmouth, MA 02747, USA

4 Department of Mathematics, Duke University, Durham, NC 27708, USA

up. A few numerical results are presented, which confirm the stability and accuracy of the proposed numerical scheme.

Keywords Functionalized Cahn–Hilliard equation · Finite difference method · Energy stability · Convergence analysis · Preconditioned steepest descent solver

Mathematics Subject Classification 35K35 · 35K55 · 65M06 · 65M12

1 Introduction

The Functionalized Cahn–Hilliard (FCH) model was first derived to describe phase separation of an amphiphilic mixture in [35]. More recent works may be found in [20,24,33,34,44,45], where, in particular, the FCH equations were extended to describe membrane bilayers [20,24], membranes and networks undergoing pearling bifurcations [7,24,27,45], the formation of pore-like and micelle network structures [33,34,45]. Consider the standard Cahn–Hilliard (CH) energy [3,9,10] given by

$$\mathcal{F}_0(\phi) = \int_\Omega \left\{ \frac{1}{4}\phi^4 - \frac{1}{2}\phi^2 + \frac{\varepsilon^2}{2}\left|\nabla\phi\right|^2 \right\} d\mathbf{x}, \tag{1.1}$$

with $\Omega \subset \mathbb{R}^D$, $D = 2$ or 3. The variable $\phi : \Omega \to \mathbb{R}$ is an order parameter, and ε is the width of interface. According to $\mathcal{F}_0$, the lowest energy "pure phase states" are $\phi = \pm 1$. We assume that $\Omega = (0, L_x) \times (0, L_y) \times (0, L_z)$ and ϕ is Ω-periodic. The Cahn–Hilliard chemical potential is the variational derivative of $\mathcal{F}_0$:

$$\mu_0 := \delta_\phi \mathcal{F}_0 = \phi^3 - \phi - \varepsilon^2 \Delta\phi. \tag{1.2}$$

Herein we consider a dimensionless energy of a binary mixture:

$$\mathcal{F}(\phi) = \frac{\varepsilon^{-2}}{2} \int_\Omega \mu_0^2 d\mathbf{x} - \eta \mathcal{F}_0(\phi), \tag{1.3}$$

where η is a parameter. When $\eta > 0$, (1.3) represents the FCH energy [24,39,44]; when $\eta < 0$, (1.3) is the Cahn–Hilliard–Willmore (CHW) energy [47,48,52]. More precisely, (1.3) represents the strong FCH energy when $\eta = O(\varepsilon^{-1})$ and weak FCH energy when $\eta = O(1)$ [24]. The FCH chemical potential is the variational derivative of $\mathcal{F}$:

$$\begin{aligned} \mu := \delta_\phi \mathcal{F} = {} & 3\varepsilon^{-2}\phi^5 - \left(4\varepsilon^{-2} + \eta\right)\phi^3 + \left(\varepsilon^{-2} + \eta\right)\phi + \varepsilon^2 \Delta^2 \phi + \left(2 + \eta\varepsilon^2\right)\Delta\phi \\ & + 6\phi\left|\nabla\phi\right|^2 - 6\nabla \cdot \left(\phi^2 \nabla\phi\right). \end{aligned} \tag{1.4}$$

Finally, the FCH equation is the conserved H^{-1} gradient flow [24,42,44]

$$\partial_t \phi = \nabla \cdot \left(M(\phi)\nabla\mu\right), \tag{1.5}$$

where $M(\phi) > 0$ is a diffusion mobility. Sufficiently regular, periodic solutions of the FCH equation (1.5) are mass conservative, that is, $d_t \int_\Omega \phi(\mathbf{x}, t)\, d\mathbf{x} = 0$, and dissipate the energy (1.3) at the rate

$$d_t \mathcal{F} = -\int_\Omega M(\phi)|\nabla\mu|^2 d\mathbf{x}.$$

The FCH equation (1.5) is a sixth-order, highly nonlinear parabolic equation. Numerical approximation of (1.5) is very challenging because of the high derivative order and the high

nonlinearity. One of the biggest challenges is to overcome the numerical stiffness encountered with time-space discretization. Roughly speaking, since the equation is sixth-order parabolic, an explicit numerical scheme is expected to encounter a severe CFL condition: $s \leq Ch^6$, with s and h the time and space step sizes. On the other hand, a fully implicit scheme, such as the backward Euler method, may still be only conditionally stable, and, very likely, will only be conditionally solvable. Ideally, one would like a scheme that preserves the time-invariant quantities of the PDE, such as mass conservation and the energy dissipation rate. The first invariant is easily maintained, while the second one is a major challenge. Often, one attempts only to design a scheme that will dissipate the free energy at the numerical level, without directly controlling the rate of dissipation. In particular, one wants $\mathcal{F}(\phi^{k+1}) \leq \mathcal{F}(\phi^k)$, where ϕ^k is the approximated phase variable at time step k, given some mild CFL condition, or no CFL condition whatever. Energy dissipation imparts some notion of norm stability for the PDE and the numerical method, as we will see. Finally, for large-scale calculations in practice, novel efficient numerical linear and nonlinear solvers have to be carefully developed. We will address this issue in the paper as well.

There have been a few previous works on the numerical approximation of the FCH equation. In [11], Chen *et al.* presented an efficient linear, first-order (in time) spectral-Galerkin method for the FCH equation. Their scheme, which utilized linear stabilization terms, is unconditionally solvable, but not necessary energy stable. Jones studied a semi-implicit numerical scheme for the FCH equation in his PhD thesis [42]. He proved the energy stability of his scheme but not the unique solvability. In a more recent work, [19], fully implicit schemes with pseudo-spectral approximation in space for the FCH equation are proposed. While the authors of [19] proved neither energy stability nor solvability, they did carry out several tests to show the accuracy and efficiency of their methods. In another work [37], Guo *et al.* presented a local discontinuous Galerkin (LDG) method to overcome the difficulty associated with the higher order spatial derivatives. Energy stability was established for the semi-discrete (time-continuous) scheme. Their fully discrete scheme was based on the time discretization in [11]. In [51] the authors developed a Runge-Kutta exponential time integration (EKR) method for the diffuse Willmore flow, an equation that is closely related to the FCH and CHW models (1.5). This method works well when $M \equiv 1$, but may need to be significantly modified otherwise. It enables one to generate high-order single-step methods, which have a significant advantage over multistep methods when the time step changes adaptively. To our knowledge, there has been no rigorous convergence analysis for the FCH model in the existing literature.

In this paper we propose and analyze an efficient computational scheme for solving the FCH equation primarily, though the theory will be applicable to the CHW equation as well. To assure both the unique solvability and unconditional energy stability, we look for a convex–concave decomposition of the physical energy $\mathcal{F}$. However, for the FCH equation (1.5), such a decomposition is highly challenging, due to a subtle fact that the expansion of $\mathcal{F}$ (see (2.5) below) contains a non-convex, non-concave term, namely, $3\int_\Omega \phi^2 |\nabla\phi|^2 \, d\mathbf{x}$. To overcome this well-known difficulty, we add and subtract a non-trivial auxiliary term in the energy functional, so that a convex–concave decomposition for the FCH energy becomes available. In turn, we derive a numerical scheme which treats the convex terms implicitly and concave terms explicitly, and the unconditional unique solvability and unconditional energy stability follow immediately. To our knowledge, the scheme proposed is the first to preserve both properties at a theoretical level.

As a result of the proposed numerical scheme, a challenging discrete nonlinear 4-Laplacian term appears at each time step in the equations. We apply an efficient preconditioned steepest descent (PSD) solver, recently proposed and analyzed in [28], to solve the nonlinear system.

The main idea is to use a linearized version of the nonlinear operator as a pre-conditioner, or in other words, as a metric for choosing the search direction. The convexity of the nonlinear energy functional assures the geometric convergence of the PSD iteration sequence. In practice, only a few constant-coefficient Poisson-like equations need to be solved at each iteration stage, which greatly improves the numerical efficiency over Newton-type methods.

Moreover, we also present a global in time H^2_{per} stability of the numerical scheme. This uniform in time bound enables us to derive the full order convergence analysis, with first order temporal accuracy and second order spatial accuracy. In addition, such a convergence is unconditional, without any requirement between the time step size s and the spatial mesh h. To the authors' knowledge, this is the first such theoretical result for the FCH/CHW model.

This article is organized as follows. In Sect. 2 we describe the convex–concave decomposition of the energy functional, formulate the numerical scheme, and establish a global in time H^2_{per} stability of the numerical scheme. In Sect. 3 we present the main results of our analysis, including the consistency, stability and convergence of our scheme. The finite difference approximation is outlined in Sect. 4, and the preconditioned steepest descent solver is formulated in Sect. 5. Subsequently, a few numerical results are presented in Sect. 6, respectively. Finally, we give some concluding remarks and some future work in Sect. 7.

2 The Numerical Scheme

2.1 Some Preliminaries

For simplicity of presentation, we denote $(\cdot, \cdot)$ as the standard L^2 inner product and $\|\cdot\|$ as the standard L^2 norm. We use the notation $H^{-1}_{\text{per}}(\Omega) = \left(H^1_{\text{per}}(\Omega)\right)^*$, and $\langle \cdot, \cdot \rangle$ is the duality paring between $H^{-1}_{\text{per}}(\Omega)$ and $H^1_{\text{per}}(\Omega)$. To define an energy for this system we need a norm on a subspace of $H^{-1}_{\text{per}}(\Omega)$. With $\mathring{L}^2(\Omega)$ denoting those function in $L^2(\Omega)$ with zero mean, we set

$$\mathring{H}^1_{\text{per}}(\Omega) = H^1_{\text{per}}(\Omega) \cap \mathring{L}^2(\Omega), \quad \mathring{H}^{-1}_{\text{per}}(\Omega) := \left\{ v \in H^{-1}_{\text{per}}(\Omega) \mid \langle v, 1 \rangle = 0 \right\}. \tag{2.1}$$

Next, we define a linear operator $\mathsf{T} : \mathring{H}^{-1}_{\text{per}}(\Omega) \to \mathring{H}^1_{\text{per}}(\Omega)$ via the following variational problem: given $\zeta \in \mathring{H}^{-1}_{\text{per}}(\Omega)$, find $\mathsf{T}(\zeta) \in \mathring{H}^1_{\text{per}}(\Omega)$ such that

$$(\nabla \mathsf{T}(\zeta), \nabla \chi) = \langle \zeta, \chi \rangle, \qquad \forall \chi \in \mathring{H}^1_{\text{per}}(\Omega). \tag{2.2}$$

T is well-defined, as guaranteed by the Riesz Representation Theorem. The following facts can be easily established [21,28].

Lemma 2.1 *Let $\zeta, \xi \in \mathring{H}^{-1}_{\text{per}}(\Omega)$ and, for such functions, we set*

$$(\zeta, \xi)_{\mathring{H}^{-1}_{\text{per}}} := (\nabla \mathsf{T}(\zeta), \nabla \mathsf{T}(\xi)) = \langle \zeta, \mathsf{T}(\xi) \rangle = \langle \xi, \mathsf{T}(\zeta) \rangle. \tag{2.3}$$

Then, $(\cdot, \cdot)_{\mathring{H}^{-1}_{\text{per}}}$ defines an inner product on $\mathring{H}^{-1}_{\text{per}}(\Omega)$, and the induced norm is equivalent to (in fact, equal to) the operator norm:

$$\|\zeta\|_{\mathring{H}^{-1}_{\text{per}}} := \sqrt{(\zeta, \zeta)_{\mathring{H}^{-1}_{\text{per}}}} = \sup_{0 \neq \chi \in \mathring{H}^1_{\text{per}}} \frac{\langle \zeta, \chi \rangle}{\|\nabla \chi\|}. \tag{2.4}$$

Consequently, we have $|\langle \zeta, \chi \rangle| \le \|\zeta\|_{\mathring{H}^{-1}_{\rm per}} \|\nabla \chi\|$, *for all* $\chi \in H^1_{\rm per}(\Omega)$ *and* $\zeta \in \mathring{H}^{-1}_{\rm per}(\Omega)$. *Furthermore, for all* $\zeta \in \mathring{L}^2(\Omega)$, *we have the Poincaré type inequality:* $\|\zeta\|_{\mathring{H}^{-1}_{\rm per}} \le C \|\zeta\|$, *for some* $C > 0$.

2.2 A Convex–Concave Energy Decomposition

For any $\phi \in H^2_{\rm per}(\Omega)$, the FCH energy in (1.3) may be expanded as

$$\mathcal{F}(\phi) = \frac{\varepsilon^{-2}}{2} \|\phi\|^6_{L^6} - \left(\varepsilon^{-2} + \frac{\eta}{4}\right) \|\phi\|^4_{L^4} + \left(\frac{\varepsilon^{-2}}{2} + \frac{\eta}{2}\right) \|\phi\|^2 + \frac{\varepsilon^2}{2} \|\Delta \phi\|^2 - \left(1 + \frac{\eta \varepsilon^2}{2}\right) \|\nabla \phi\|^2 + 3 \int_\Omega \phi^2 |\nabla \phi|^2 \, d\mathbf{x}. \tag{2.5}$$

To design a numerical scheme with unconditional energy stability, we look for a convex–concave decomposition of the FCH energy. However, unlike the energies for the Allen–Cahn [30], Cahn–Hilliard and its variants [4,13,21,26,31,36], phase field crystal (PFC) [50,53], epitaxial thin film [12,49] equations, a direct application the convex–concave decomposition is not available the FCH energy (1.3). The main difficulty is associated with the last term in (2.5),

$$\mathcal{G}(\phi) := \int_\Omega 3\phi^2 |\nabla \phi|^2 \, d\mathbf{x}, \tag{2.6}$$

which is neither convex nor concave. To overcome this difficulty, we perform a careful analysis for the following energy functional:

$$\mathcal{H}(\phi) := \int_\Omega \left(A(\phi^4 + |\nabla \phi|^4) + 3\phi^2 |\nabla \phi|^2 \right) d\mathbf{x}. \tag{2.7}$$

Lemma 2.2 $\mathcal{H} : W^{1,4}_{\rm per}(\Omega) \to \mathbb{R}$ *is convex provided that* $A \ge 1$.

Proof We denote $g(\phi) := 3\phi^2 |\nabla \phi|^2$ and $h(\phi) := A(\phi^4 + |\nabla \phi|^4) + g(\phi)$, so that $\mathcal{G}(\phi) = \int_\Omega g(\phi) \, d\mathbf{x}$ and $\mathcal{H}(\phi) = \int_\Omega h(\phi) \, d\mathbf{x}$. Based on the pointwise inequalities,

$$\left(\frac{\phi_1 + \phi_2}{2}\right)^2 \le \frac{\phi_1^2 + \phi_2^2}{2}, \quad \left|\nabla \left(\frac{\phi_1 + \phi_2}{2}\right)\right|^2 \le \frac{|\nabla \phi_1|^2 + |\nabla \phi_2|^2}{2}, \quad \forall \phi_1, \, \phi_2,$$

which come from the convexity of $q_2(x) = x^2$ and $r_2(\boldsymbol{x}) = \boldsymbol{x} \cdot \boldsymbol{x}$, we find that

$$g\left(\frac{\phi_1 + \phi_2}{2}\right) = 3\left(\frac{\phi_1 + \phi_2}{2}\right)^2 \left|\nabla \left(\frac{\phi_1 + \phi_2}{2}\right)\right|^2 \le 3 \frac{\phi_1^2 + \phi_2^2}{2} \cdot \frac{|\nabla \phi_1|^2 + |\nabla \phi_2|^2}{2}.$$

A careful comparison with $\frac{g(\phi_1) + g(\phi_2)}{2} = \frac{3\phi_1^2 |\nabla \phi_1|^2 + 3\phi_2^2 |\nabla \phi_2|^2}{2}$ shows that

$$\begin{aligned} \frac{g(\phi_1) + g(\phi_2)}{2} - g\left(\frac{\phi_1 + \phi_2}{2}\right) &\ge \frac{3(\phi_1^2 - \phi_2^2)(|\nabla \phi_1|^2 - |\nabla \phi_2|^2)}{4} \\ &\ge -\frac{3}{8}\left((\phi_1^2 - \phi_2^2)^2 + (|\nabla \phi_1|^2 - |\nabla \phi_2|^2)^2\right). \end{aligned} \tag{2.8}$$

Meanwhile, the convexity of $q_4(x) = x^4$ and $r_4(\boldsymbol{x}) = |\boldsymbol{x}|^4$ indicates the following inequalities:

$$\frac{\phi_1^4 + \phi_2^4}{2} - \left(\frac{\phi_1 + \phi_2}{2}\right)^4 \ge \frac{3}{8}(\phi_1^4 + \phi_2^4 - 2\phi_1^2 \phi_2^2) = \frac{3}{8}(\phi_1^2 - \phi_2^2)^2, \tag{2.9}$$

and

$$\frac{|\nabla\phi_1|^4+|\nabla\phi_2|^4}{2}-\left|\nabla\left(\frac{\phi_1+\phi_2}{2}\right)\right|^4 \geq \frac{3}{8}(|\nabla\phi_1|^4+|\nabla\phi_2|^4-2|\nabla\phi_1|^2\cdot|\nabla\phi_2|^2)$$
$$=\frac{3}{8}(|\nabla\phi_1|^2-|\nabla\phi_2|^2)^2. \tag{2.10}$$

A combination of (2.8), (2.9) and (2.10) implies that

$$\frac{h(\phi_1)+h(\phi_2)}{2}-h\left(\frac{\phi_1+\phi_2}{2}\right)\geq 0, \quad \forall\phi_1,\ \phi_2,$$

provided that $A \geq 1$. As a result, an integration over Ω leads to the following fact:

$$\frac{\mathcal{H}(\phi_1)+\mathcal{H}(\phi_2)}{2}-\mathcal{H}\left(\frac{\phi_1+\phi_2}{2}\right)\geq 0, \quad \forall\phi_1,\ \phi_2, \quad \text{if } A\geq 1.$$

The convexity of H is assured under the condition $A \geq 1$. □

Corollary 2.3 *The energy $\mathcal{F}: H^2_{\text{per}}(\Omega)\to\mathbb{R}$ possesses a convex–concave decomposition:*

$$\mathcal{F}(\phi)=\mathcal{F}_c(\phi)-\mathcal{F}_e(\phi), \tag{2.11}$$

with

$$\mathcal{F}_c(\phi):=\int_\Omega\left\{\frac{\varepsilon^{-2}}{2}\phi^6+\left(\frac{\varepsilon^{-2}}{2}+\frac{\eta}{2}\right)\phi^2+\frac{\varepsilon^2}{2}(\Delta\phi)^2+A(\phi^4+|\nabla\phi|^4)+3\phi^2|\nabla\phi|^2\right\}d\mathbf{x}, \tag{2.12}$$

and

$$\mathcal{F}_e(\phi):=\int_\Omega\left\{\left(\epsilon^{-2}+\frac{\eta}{4}\right)\phi^4+\left(1+\frac{\eta\varepsilon^2}{2}\right)|\nabla\phi|^2+A(\phi^4+|\nabla\phi|^4)\right\}d\mathbf{x}, \tag{2.13}$$

where both $\mathcal{F}_c, \mathcal{F}_e: H^2_{\text{per}}(\Omega)\to\mathbb{R}$ are strictly convex provided $A\geq 1$.

We recall the following proposition from [53]:

Proposition 2.4 *Suppose that $\phi,\ \psi\in H^4_{\text{per}}(\Omega)$ and that $\mathcal{F}$ admits a (not necessarily unique) convex–concave decomposiiton into $\mathcal{F}=\mathcal{F}_c-\mathcal{F}_e$ then*

$$\mathcal{F}(\phi)-\mathcal{F}(\psi)\leq\left(\delta_\phi\mathcal{F}_c(\phi)-\delta_\phi\mathcal{F}_e(\psi),\phi-\psi\right). \tag{2.14}$$

If $\phi,\ \psi\in H^2_{\text{per}}(\Omega)$ only, then (2.14) can be interpreted in the weak sense.

2.3 The Proposed Numerical Scheme

Based on the decomposition in (2.12) and (2.13) for the physical energy $\mathcal{F}(\phi)$, we consider the following semi-implicit, first-order-in-time numerical scheme:

$$\phi^{k+1}-\phi^k=s\nabla\cdot\left(M(\phi^k)\nabla\tilde{\mu}\right),\quad \tilde{\mu}\left(\phi^{k+1},\phi^k\right):=\delta_\phi\mathcal{F}_c(\phi^{k+1})-\delta_\phi\mathcal{F}_e(\phi^k), \tag{2.15}$$

where, precisely,

$$\tilde{\mu}\left(\phi^{k+1},\phi^k\right)=3\varepsilon^{-2}(\phi^{k+1})^5+4A(\phi^{k+1})^3+(\varepsilon^{-2}+\eta)\phi^{k+1}+\varepsilon^2\Delta^2\phi^{k+1}$$
$$+6\phi^{k+1}\left|\nabla\phi^{k+1}\right|^2-6\nabla\cdot\left((\phi^{k+1})^2\nabla\phi^{k+1}\right)-4A\nabla\cdot\left(|\nabla\phi^{k+1}|^2\nabla\phi^{k+1}\right) \tag{2.16}$$

$$- (4\varepsilon^{-2} + \eta)(\phi^k)^3 + (2 + \eta\varepsilon^2)\Delta\phi^k - 4A(\phi^k)^3 + 4A\nabla \cdot \left(|\nabla\phi^k|^2\nabla\phi^k\right).$$

The scheme may be expressed in a weak form as follows: find the pair $(\phi, \mu) \in H^2_{\text{per}}(\Omega) \times H^1_{\text{per}}(\Omega)$ such that

$$(\phi, \nu) + s(M\nabla\mu, \nabla\nu) = (g, \nu), \tag{2.17}$$

$$\left(3\varepsilon^{-2}\phi^5 + 4A\phi^3 + (\varepsilon^{-2} + \eta)\phi, \psi\right) + \varepsilon^2(\Delta\phi, \Delta\psi) + 6(\phi\,|\nabla\phi|^2, \psi) \tag{2.18}$$

$$+ 6\left(\phi^2\nabla\phi, \nabla\psi\right) + 4A\left(|\nabla\phi|^2\nabla\phi, \nabla\psi\right) - (\mu, \psi) = (f, \psi), \tag{2.19}$$

where $g = \phi^k$, $M = M(\phi^k)$, and

$$f = \delta_\phi \mathcal{F}_e(\phi^k) = (4\varepsilon^{-2} + \eta)(\phi^k)^3 - (2 + \eta\varepsilon^2)\Delta\phi^k + 4A(\phi^k)^3 - 4A\nabla \cdot \left(|\nabla\phi^k|^2\nabla\phi^k\right).$$

Observe that, if $\phi^k \in H^2_{\text{per}}(\Omega)$ is given, we have $g,\ f \in L^2_{\text{per}}(\Omega) = L^2(\Omega)$.

Theorem 2.5 *The proposed numerical scheme (2.15) is uniquely solvable and unconditionally energy stable: $\mathcal{F}(\phi^{k+1}) \le \mathcal{F}(\phi^k)$. In particular, if $\phi^k \in H^2_{\text{per}}(\Omega)$, then $\phi^{k+1} \in H^2_{\text{per}}(\Omega)$.*

Proof The existence and unique solvability follows from standard convexity analyses. For the stability, let $\phi = \phi^{k+1}$ and $\psi = \phi^k$ in (2.14) to find

$$\begin{aligned}\mathcal{F}(\phi^{k+1}) - \mathcal{F}(\phi^k) &\le \left(\delta_\phi\mathcal{F}_c(\phi^{k+1}) - \delta_\phi\mathcal{F}_e(\phi^k), \phi^{k+1} - \phi^k\right)\\ &= s\left(\tilde{\mu}, \nabla\cdot\left(M(\phi^k)\nabla\tilde{\mu}\right)\right) = -s\left(\nabla\tilde{\mu}, M(\phi^k)\nabla\tilde{\mu}\right) \le 0,\end{aligned}$$

where we have interpreted the right-hand-side of (2.14) in the weak sense. □

Remark 2.6 A slightly simpler numerical algorithm than ours was studied in Jones' thesis [42]:

$$\phi^{k+1} - \phi^k = s\nabla\cdot\left(M(\phi^k)\nabla\hat{\mu}\right), \tag{2.20}$$

$$\begin{aligned}\hat{\mu}\left(\phi^{k+1}, \phi^k\right) = {}& 3\varepsilon^{-2}(\phi^{k+1})^5 + (\varepsilon^{-2} + \eta)\phi^{k+1} + \varepsilon^2\Delta^2\phi^{k+1} - (4\varepsilon^{-2} + \eta)(\phi^k)^3\\ &+ (2 + \eta\varepsilon^2)\Delta\phi^k + 6\phi^{k+1}|\nabla\phi^k|^2 - 6\nabla\cdot\left((\phi^{k+1})^2\nabla\phi^{k+1}\right).\end{aligned} \tag{2.21}$$

In other words, a semi-implicit treatment is applied to the non-convex, non-concave energy term (2.6). A careful analysis shows that, if the numerical algorithm (2.20)–(2.21) is solvable, then it is energy stable. It was proved in [42] that this nonlinear numerical scheme has at most one solution. However, for the numerical method proposed in [42], the solvability issue has not been fully theoretically justified.

To ensure both the unconditional unique solvability and unconditional energy stability of our scheme, we have to add and subtract two auxiliary terms in the energy decomposition, as given by (2.12)–(2.13); this is the first numerical approach to preserve both solvability and stability properties, unconditionally for the FCH/CHW models.

Remark 2.7 In addition to the first order convex splitting schemes, various second order accurate energy stable schemes have been reported in recent years, such as the ones for the Cahn–Hilliard [22,23,36], phase field crystal (PFC) [5,6,25,40], epitaxial thin film [14,43,46], etc. We notice that most of these second order numerical approaches are based on the Crank–Nicolson temporal approximation. On the other hand, a direct extension of the

first order scheme (2.15) to the Crank–Nicolson version is not directly available for the FCH equation (1.5). Such a difficulty comes from the non-convex, non-concave term $\mathcal{G}(\phi)$ in (2.6), since an application of Crank–Nicolson approach leads to a difficulty to justify the unique solvability.

Instead, we believe that the idea of a modified 2nd order BDF approach, which has been successfully applied to the Cahn–Hilliard [54] and the epitaxial thin film [29] models, could be similarly used to derive a unique solvable, energy stable, second order accurate numerical scheme to the FCH/CHW model. Of course, many more technical details have to be involved with a much more careful way, due to the appearance of the non-convex, non-concave term $\mathcal{G}(\phi)$, as well as the subtle fact that the concave energy part contains a few highly nonlinear terms. The details have to left to the future works.

2.4 Global-in-Time H^2_{per} Stability of the Numerical Scheme

For simplicity, we will take the mobility $M \equiv 1$ in the remainder of the paper.

Lemma 2.8 *There are constants $C_0, C_1 > 0$ such that, for all $\phi \in H^2_{\text{per}}(\Omega)$,*

$$\frac{\varepsilon^{-2}}{6} \|\phi\|_{L^6}^6 + C_0 \varepsilon^2 \|\phi\|_{H^2_{\text{per}}}^2 \le \mathcal{F}(\phi) + C_1. \tag{2.22}$$

Proof For the concave diffusion term in (2.5), an application of Cauchy's inequality shows that

$$\|\nabla\phi\|^2 = \int_\Omega \phi \cdot \Delta\phi \, d\mathbf{x} \le \|\phi\| \cdot \|\Delta\phi\| \le \frac{\varepsilon^2}{4\left(1 + \frac{\eta\varepsilon^2}{2}\right)} \|\Delta\phi\|^2 + \frac{1 + \frac{\eta\varepsilon^2}{2}}{\varepsilon^2} \|\phi\|^2, \quad \forall\, \eta > 0. \tag{2.23}$$

Then we obtain

$$\left(1 + \frac{\eta\varepsilon^2}{2}\right) \|\nabla\phi\|^2 \le \frac{\varepsilon^2}{4} \|\Delta\phi\|^2 + C_2 \|\phi\|^2, \tag{2.24}$$

with $C_2 := (1 + \frac{\eta\varepsilon^2}{2})^2 \varepsilon^{-2} = O(\varepsilon^{-2})$. Applications of Hölder's inequality imply that

$$\|\phi\|_{L^6} \ge \frac{1}{|\Omega|^{1/12}} \|\phi\|_{L^4}, \quad \|\phi\|_{L^6} \ge \frac{1}{|\Omega|^{1/3}} \|\phi\|.$$

Now, define $C_3 := C_2 - \left(\frac{\varepsilon^{-2}}{2} + \frac{\eta}{2}\right) + 1 > 0$; we note that $C_3 = O(\varepsilon^{-2})$. As a consequence of the last two inequalities, we get

$$\frac{1}{6} \|\phi\|_{L^6}^6 \ge \frac{1}{6|\Omega|^{1/2}} \|\phi\|_{L^4}^6 \ge \left(1 + \frac{\eta\varepsilon^2}{4}\right) \|\phi\|_{L^4}^4 - C_4, \tag{2.25}$$

$$\frac{1}{6} \|\phi\|_{L^6}^6 \ge \frac{1}{6|\Omega|^2} \|\phi\|^6 \ge \varepsilon^2 C_3 \|\phi\|^2 - C_5, \tag{2.26}$$

for some constants $C_4, C_5 > 0$, which are of order 1, where Young's inequality was repeated applied. Therefore, a combination of (2.5), (2.24), (2.25) and (2.26) yields

$$\begin{aligned} \mathcal{F}(\phi) &\ge \frac{\varepsilon^{-2}}{6} \|\phi\|_{L^6}^6 + \|\phi\|^2 + \frac{\varepsilon^2}{4} \|\Delta\phi\|^2 - C_1, \\ &\ge \frac{\varepsilon^{-2}}{6} \|\phi\|_{L^6}^6 + C_0 \varepsilon^2 \|\phi\|_{H^2_{\text{per}}}^2 - C_1, \end{aligned} \tag{2.27}$$

where $C_1 := \varepsilon^{-2}(C_4 + C_5) = O(\varepsilon^{-2})$ and the elliptic regularity estimate $\|\phi\|_{H^2}^2 \le C_0(\|\phi\|^2 + \|\Delta\phi\|^2)$ was applied in the second step. □

Corollary 2.9 *Suppose that $\phi_0 \in H^2_{\text{per}}(\Omega)$. For any positive integer k, we have*

$$\left\|\phi^k\right\|_{H^2_{\text{per}}} \le C_6 := \frac{\mathcal{F}(\phi^0) + C_1}{C_0\varepsilon^2}. \tag{2.28}$$

Proof The unconditional energy stability in Theorem 2.5 implies that, for any positive integer k,

$$\mathcal{F}(\phi^k) \le \mathcal{F}(\phi^0). \tag{2.29}$$

A combination of (2.22) and (2.29) yields the result. □

Remark 2.10 Note that the constant C_6 is independent of k and s, but does depends on ε. In particular, $C_6 = O(\varepsilon^{-4})$.

3 Convergence Analysis

3.1 Main Result

We introduce the regularity class

$$\mathcal{R}_1 := C^2([0,T]; C^0_{\text{per}}(\Omega)) \cap C^1([0,T]; C^4_{\text{per}}(\Omega)) \cap L^\infty([0,T]; C^6_{\text{per}}(\Omega)). \tag{3.1}$$

We have the following convergence result.

Theorem 3.1 *Let $\Phi \in \mathcal{R}_1$ be the exact periodic solution of the FCH equation (1.5) with the initial data $\Phi(0) = \phi_0 \in H^2_{\text{per}}(\Omega)$. Suppose ϕ is the space-continuous numerical solution of (2.15). Then the following error estimate is valid:*

$$\|\Phi - \phi\|_{\ell^\infty(0,T;\mathring{H}^{-1}_{\text{per}})} + \|\Phi - \phi\|_{\ell^2(0,T;H^2_{\text{per}})} \le Cs, \tag{3.2}$$

where the constant $C > 0$ is independent of s but depends on the regularity of the exact solution.

3.2 Proof of the Main Result

3.2.1 Consistency Analysis

The theorem is proved in a number of steps. Define $\Phi^k = \Phi(\cdot, t_k)$. A detailed Taylor expansion implies the following truncation error:

$$\begin{aligned}\frac{\Phi^{k+1} - \Phi^k}{s} = \Delta\Big(& 3\varepsilon^{-2}(\Phi^{k+1})^5 - (4\varepsilon^{-2} + \eta)(\Phi^k)^3 + (\varepsilon^{-2} + \eta)\Phi^{k+1} + \varepsilon^2\Delta^2\Phi^{k+1} \\ & + (2 + \eta\varepsilon^2)\Delta\Phi^k + 6\Phi^{k+1}\left|\nabla\Phi^{k+1}\right|^2 - 6\nabla\cdot\left((\Phi^{k+1})^2\nabla\Phi^{k+1}\right) \\ & + 4A(\Phi^{k+1})^3 - 4A\nabla\cdot\left(|\nabla\Phi^{k+1}|^2\nabla\Phi^{k+1}\right) \\ & - 4A(\Phi^k)^3 + 4A\nabla\cdot\left(|\nabla\Phi^k|^2\nabla\Phi^k\right)\Big) + \tau^k,\end{aligned} \tag{3.3}$$

with $\|\tau^k\| \le Cs$. Consequently, with an introduction of the error function

$$e^k = \Phi^k - \phi^k, \quad \forall k \ge 0, \tag{3.4}$$

we get the following evolutionary equation, by subtracting (2.16) from (3.3):

$$\begin{aligned}
\frac{e^{k+1}-e^k}{s} &= \Delta\Big(3\varepsilon^{-2}\left((\Phi^{k+1})^4+(\Phi^{k+1})^3\phi^{k+1}+(\Phi^{k+1})^2(\phi^{k+1})^2+\Phi^{k+1}(\phi^{k+1})^3+(\phi^{k+1})^4\right)e^{k+1}\\
&\quad -(4\varepsilon^{-2}+\eta+4A)\left((\Phi^k)^2+\Phi^k\phi^k+(\phi^k)^2\right)e^k+(\varepsilon^{-2}+\eta)e^{k+1}+\varepsilon^2\Delta^2 e^{k+1}\\
&\quad +(2+\eta\varepsilon^2)\Delta e^k+6e^{k+1}\left|\nabla\Phi^{k+1}\right|^2+6\phi^{k+1}\left(\nabla(\Phi^{k+1}+\phi^{k+1})\cdot\nabla e^{k+1}\right)\\
&\quad -6\nabla\cdot\left((\Phi^{k+1}+\phi^{k+1})e^{k+1}\nabla\Phi^{k+1}+(\phi^{k+1})^2\nabla e^{k+1}\right)\\
&\quad +4A\left((\Phi^{k+1})^2+\Phi^{k+1}\phi^{k+1}+(\phi^{k+1})^2\right)e^{k+1}\\
&\quad -4A\nabla\cdot\left((\nabla(\Phi^{k+1}+\phi^{k+1})\cdot\nabla e^{k+1})\nabla\Phi^{k+1}+|\nabla\phi^{k+1}|^2\nabla e^{k+1}\right)\\
&\quad +4A\nabla\cdot\left((\nabla(\Phi^k+\phi^k)\cdot\nabla e^k)\nabla\Phi^k+|\nabla\phi^k|^2\nabla e^k\right)\Big)+\tau^k.
\end{aligned} \tag{3.5}$$

In addition, from the PDE analysis for the FCH equation and the global in time H^2_{per} stability (2.28) for the numerical solution, we also get the L^∞, $W^{1,6}$ and H^2_{per} bounds for both the exact solution and numerical solution, uniform in time:

$$\|\Phi^k\|_{L^\infty},\ \|\Phi^k\|_{W^{1,6}},\ \|\Phi^k\|_{H^2_{\text{per}}} \le C_7, \quad \|\phi^k\|_{L^\infty},\ \|\phi^k\|_{W^{1,6}},\ \|\phi^k\|_{H^2_{\text{per}}} \le C_7, \quad \forall k \ge 0, \tag{3.6}$$

where the 3-D embeddings of H^2_{per} into L^∞ and into $W^{1,6}$ have been applied. Note that C_7 and C_8 are time independent constants, that depend on ε as $O(\varepsilon^{-4})$.

3.2.2 Stability and Convergence Analysis

First, we recall that the exact solution to the FCH equation (1.5) is mass conservative:

$$\int_\Omega \Phi(\mathbf{x},t)\,d\mathbf{x} \equiv \int_\Omega \Phi(\mathbf{x},0)\,d\mathbf{x}, \quad \forall t > 0.$$

On the other hand, the numerical solution (2.15) is also mass conservative. In turn, we conclude that the numerical error function $e^k \in \mathring{H}^2_{\text{per}}(\Omega)$:

$$\overline{e^k} := \int_\Omega e^k\,d\mathbf{x} = \int_\Omega e^0 = 0, \quad \text{since } e^0 \equiv 0.$$

Consequently, we define $\psi^k := (-\Delta)^{-1}e^k \in \mathring{H}^{-1}_{\text{per}}(\Omega)$ as

$$-\Delta\psi^k = e^k, \quad \text{with} \int_\Omega \psi^k\,d\mathbf{x} = 0.$$

Define I_i, $i = 1, \cdots, 10$ by

$$\begin{aligned}
I_1 := -6\varepsilon^{-2}s\int_\Omega &\Big((\Phi^{k+1})^4+(\Phi^{k+1})^3\phi^{k+1}+(\Phi^{k+1})^2(\phi^{k+1})^2\\
&+\Phi^{k+1}(\phi^{k+1})^3+(\phi^{k+1})^4\Big)\left|e^{k+1}\right|^2 d\mathbf{x},
\end{aligned}$$

$$
\begin{aligned}
I_2 &:= -8As \int_\Omega \left((\Phi^{k+1})^2 + \Phi^{k+1}\phi^{k+1} + (\phi^{k+1})^2 \right) \left| e^{k+1} \right|^2 d\mathbf{x}, \\
I_3 &:= 2(2+\eta\varepsilon^2)s(\nabla e^k, \nabla e^{k+1}), \\
I_4 &:= 2(4\varepsilon^{-2} + \eta + 4A)s \int_\Omega \left((\Phi^k)^2 + \Phi^k\phi^k + (\phi^k)^2 \right) e^k e^{k+1} d\mathbf{x}, \\
I_5 &:= -12s \int_\Omega |\nabla \Phi^{k+1}|^2 (e^{k+1})^2 d\mathbf{x}, \\
I_6 &:= -12s \int_\Omega \phi^{k+1} \left(\nabla(\Phi^{k+1} + \phi^{k+1}) \cdot \nabla e^{k+1} \right) e^{k+1} d\mathbf{x}, \\
I_7 &:= -12s \left((\Phi^{k+1} + \phi^{k+1}) e^{k+1} \nabla \Phi^{k+1} + (\phi^{k+1})^2 \nabla e^{k+1}, \nabla e^{k+1} \right), \\
I_8 &:= -8As \left((\nabla(\Phi^{k+1} + \phi^{k+1}) \cdot \nabla e^{k+1}) \nabla \Phi^{k+1} + |\nabla \phi^{k+1}|^2 \nabla e^{k+1}, \nabla e^{k+1} \right), \\
I_9 &:= 8As \left((\nabla(\Phi^k + \phi^k) \cdot \nabla e^k) \nabla \Phi^k + |\nabla \phi^k|^2 \nabla e^k, \nabla e^{k+1} \right), \\
I_{10} &:= -2s(\tau^k, e^{k+1}).
\end{aligned}
$$

Taking an L^2 inner product of the error equation (3.5) with $2\psi^k$ gives

$$
\|e^{k+1}\|^2_{\mathring{H}^{-1}_{\text{per}}} - \|e^k\|^2_{\mathring{H}^{-1}_{\text{per}}} + \|e^{k+1} - e^k\|^2_{\mathring{H}^{-1}_{\text{per}}} + 2(\varepsilon^{-2} + \eta)s\|e^{k+1}\|^2 + 2\varepsilon^2 s\|\Delta e^{k+1}\|^2 = \sum_{i=1}^{10} I_i, \tag{3.7}
$$

where integration-by-parts has been repeatedly applied.

The local truncation error term I_{10} can be bounded by the Cauchy inequality:

$$
-2(\tau^k, e^{k+1}) \le 2\|\tau^k\| \cdot \|e^{k+1}\| \le \|\tau^k\|^2 + \|e^{k+1}\|^2. \tag{3.8}
$$

Meanwhile, an application of an interpolated Sobolev inequality shows that

$$
\|e^{k+1}\| \le C_8 \|e^{k+1}\|^{2/3}_{\mathring{H}^{-1}_{\text{per}}} \cdot \|e^{k+1}\|^{1/3}_{\mathring{H}^2_{\text{per}}} \le C_9 \|e^{k+1}\|^{2/3}_{\mathring{H}^{-1}_{\text{per}}} \cdot \|\Delta e^{k+1}\|^{1/3}, \tag{3.9}
$$

where a standard estimate of elliptic regularity was applied at the second step, considering the fact that $\overline{e^{k+1}} = 0$. Subsequently, an application of Young's inequality gives

$$
\|e^{k+1}\|^2 \le C_{10}\varepsilon^{-1}\|e^{k+1}\|^2_{\mathring{H}^{-1}_{\text{per}}} + \frac{\varepsilon^2}{8}\|\Delta e^{k+1}\|^2,
$$

and its combination with (3.8) yields

$$
-2(\tau^k, e^{k+1}) \le \|\tau^k\|^2 + C_{10}\varepsilon^{-1}\|e^{k+1}\|^2_{\mathring{H}^{-1}_{\text{per}}} + \frac{\varepsilon^2}{8}\|\Delta e^{k+1}\|^2. \tag{3.10}
$$

The first integral term I_1 turns out to be non-positive,

$$
I_1 \le 0, \tag{3.11}
$$

due to the fact that

$$
(\Phi^{k+1})^4 + (\Phi^{k+1})^3\phi^{k+1} + (\Phi^{k+1})^2(\phi^{k+1})^2 + \Phi^{k+1}(\phi^{k+1})^3 + (\phi^{k+1})^4 \ge 0.
$$

Since $(\Phi^{k+1})^2 + \Phi^{k+1}\phi^{k+1} + (\phi^{k+1})^2 \ge 0$, similar estimates can be derived for I_2 and I_5:

$$
I_2 = -8As \int_\Omega \left((\Phi^{k+1})^2 + \Phi^{k+1}\phi^{k+1} + (\phi^{k+1})^2 \right) \left| e^{k+1} \right|^2 d\mathbf{x} \le 0, \tag{3.12}
$$

$$I_5 = -12s \int_\Omega |\nabla \Phi^{k+1}|^2 (e^{k+1})^2 d\mathbf{x} \le 0. \tag{3.13}$$

For the term I_3, we denote $C_{11} = 2 + \eta\varepsilon^2$ and observe that

$$I_3 = 2C_{11} s(\nabla e^k, \nabla e^{k+1}) \le C_{11} s(\|\nabla e^k\|^2 + \|\nabla e^{k+1}\|^2). \tag{3.14}$$

Meanwhile, a similar estimate as (3.9) could be carried out to bound $\|\nabla e^{k+1}\|$:

$$\|\nabla e^{k+1}\| \le C_{12} \|e^{k+1}\|_{\mathring{H}^{-1}_{\text{per}}}^{1/3} \cdot \|e^{k+1}\|_{H^2_{\text{per}}}^{2/3} \le C_{13} \|e^{k+1}\|_{\mathring{H}^{-1}_{\text{per}}}^{1/3} \cdot \|\Delta e^{k+1}\|^{2/3}, \tag{3.15}$$

so that an application of Young's inequality leads to

$$\|\nabla e^{k+1}\|^2 \le C_{14} \varepsilon^{-4} \|e^{k+1}\|_{\mathring{H}^{-1}_{\text{per}}}^2 + \frac{\varepsilon^2}{8C_{11}} \|\Delta e^{k+1}\|^2. \tag{3.16}$$

The term $\|\nabla e^k\|$ can be bounded in the same fashion:

$$\|\nabla e^k\|^2 \le C_{15} \varepsilon^{-4} \|e^k\|_{\mathring{H}^{-1}_{\text{per}}}^2 + \frac{\varepsilon^2}{8C_{11}} \|\Delta e^k\|^2. \tag{3.17}$$

Substituting (3.16) and (3.17) into (3.14), we get

$$I_3 \le C_{16} s \left(\|e^{k+1}\|_{\mathring{H}^{-1}_{\text{per}}}^2 + \|e^k\|_{\mathring{H}^{-1}_{\text{per}}}^2 \right) + \frac{\varepsilon^2}{8} s \left(\|\Delta e^{k+1}\|^2 + \|\Delta e^k\|^2 \right). \tag{3.18}$$

For the term I_4, we denote $C_{17} = 4\varepsilon^{-2} + \eta + 4A$. By the L^∞ bound in (3.6) for both the exact and numerical solutions, we see that

$$\|(\Phi^k)^2 + \Phi^k \phi^k + (\phi^k)^2\|_{L^\infty} \le 3C_7^2. \tag{3.19}$$

This in turn implies that

$$\begin{aligned} I_4 &\le 2C_{17} s \|(\Phi^k)^2 + \Phi^k \phi^k + (\phi^k)^2\|_{L^\infty} \cdot \|e^k\| \cdot \|e^{k+1}\| \\ &\le 6C_{17} C_7^2 s \|e^k\| \cdot \|e^{k+1}\| \le 3C_{17} C_7^2 s (\|e^k\|^2 + \|e^{k+1}\|^2). \end{aligned} \tag{3.20}$$

Meanwhile, the estimate (3.10) can be performed with alternate coefficients, so that the following inequalities are available:

$$\|e^j\|^2 \le C_{18} \|e^j\|_{\mathring{H}^{-1}_{\text{per}}}^2 + \frac{\varepsilon^2}{24 C_{17} C_7^2} \|\Delta e^j\|^2, \quad \text{for } j = k, k+1. \tag{3.21}$$

Subsequently, its combination with (3.20) yields

$$I_4 \le C_{19} s \left(\|e^k\|_{\mathring{H}^{-1}_{\text{per}}}^2 + \|e^{k+1}\|_{\mathring{H}^{-1}_{\text{per}}}^2 \right) + \frac{\varepsilon^2}{8} s \left(\|\Delta e^{k+1}\|^2 + \|\Delta e^k\|^2 \right). \tag{3.22}$$

For the term I_6, we start from an application of Hölder inequality:

$$\begin{aligned} I_6 &= -12s \int_\Omega \phi^{k+1} \left(\nabla(\Phi^{k+1} + \phi^{k+1}) \cdot \nabla e^{k+1} \right) e^{k+1} d\mathbf{x} \\ &\le C_{20} s \|\phi^{k+1}\|_{L^\infty} \cdot \left(\|\nabla \Phi^{k+1}\|_{L^6} + \|\nabla \phi^{k+1}\|_{L^6} \right) \cdot \|\nabla e^{k+1}\|_{L^{3/2}} \cdot \|e^{k+1}\|_{L^6} \\ &\le C_{21} C_7^2 s \cdot \|\nabla e^{k+1}\|_{L^{3/2}} \cdot \|e^{k+1}\|_{L^6}, \end{aligned} \tag{3.23}$$

in which the L^∞ and $W^{1,6}$ stability bounds for the exact and numerical solutions were recalled in the second step of (3.6). Moreover, the first term $\|\nabla e^{k+1}\|_{L^{3/2}}$ can be bounded in the following way:

$$\|\nabla e^{k+1}\|_{L^{3/2}} \le C_{22}\|\nabla e^{k+1}\| \le C_{23}\|e^{k+1}\|_{\mathring{H}^{-1}_{\text{per}}}^{1/3} \cdot \|\Delta e^{k+1}\|^{2/3}, \tag{3.24}$$

with an earlier estimate (3.15) recalled. For the second term $\|e^{k+1}\|_{L^6}$, a 3-D Sobolev embedding could be applied so that

$$\|e^{k+1}\|_{L^6} \le C_{24}\|\nabla e^{k+1}\| \le C_{25}\|e^{k+1}\|_{\mathring{H}^{-1}_{\text{per}}}^{1/3} \cdot \|\Delta e^{k+1}\|^{2/3}. \tag{3.25}$$

We also note that the zero-mean property for e^{k+1} was used in the first step. Therefore, a combination of (3.23)–(3.25) results in

$$I_6 \le C_{26}C_7^2 s\|e^{k+1}\|_{\mathring{H}^{-1}_{\text{per}}}^{2/3} \cdot \|\Delta e^{k+1}\|^{4/3} \le C_{27}s\|e^{k+1}\|_{\mathring{H}^{-1}_{\text{per}}}^2 + \frac{\varepsilon^2}{8}s\|\Delta e^{k+1}\|^2, \tag{3.26}$$

with the Young's inequality applied in the last step.

For the term I_7, we decompose it into two parts: $I_7 = I_{7,1} + I_{7,2}$, with

$$I_{7,1} = -12s\left((\Phi^{k+1} + \phi^{k+1})e^{k+1}\nabla\Phi^{k+1}, \nabla e^{k+1}\right), \tag{3.27}$$

$$I_{7,2} = -12s\left((\phi^{k+1})^2\nabla e^{k+1}, \nabla e^{k+1}\right). \tag{3.28}$$

It is clear that the second part is always non-positive:

$$I_{7,2} = -12s\int_\Omega (\phi^{k+1})^2|\nabla e^{k+1}|^2 d\mathbf{x} \le 0. \tag{3.29}$$

For the first part, an application of Hölder inequality shows that

$$\begin{aligned} I_{7,1} &\le C_{28}s(\|\Phi^{k+1}\|_{L^\infty} + \|\phi^{k+1}\|_{L^\infty}) \cdot \|\nabla\Phi^{k+1}\|_{L^6} \cdot \|\nabla e^{k+1}\|_{L^{3/2}} \cdot \|e^{k+1}\|_{L^6} \\ &\le C_{29}C_7^2 s\|\nabla e^{k+1}\|_{L^{3/2}} \cdot \|e^{k+1}\|_{L^6}. \end{aligned} \tag{3.30}$$

Again, the L^∞ and $W^{1,6}$ bounds (3.6) for the exact and numerical solutions were recalled in the second step. Furthermore, by repeating the same analyses as (3.24)–(3.25), we are able to arrive at the following estimate, similar to (3.26):

$$I_{7,1} \le C_{30}C_7^2 s \cdot \|e^{k+1}\|_{\mathring{H}^{-1}_{\text{per}}}^{1/3} \cdot \|\Delta e^{k+1}\|^{2/3} \le C_{31}s\|e^{k+1}\|_{\mathring{H}^{-1}_{\text{per}}}^2 + \frac{\varepsilon^2}{8}s\|\Delta e^{k+1}\|^2. \tag{3.31}$$

Consequently, a combination of (3.28), (3.29) and (3.31) leads to

$$I_7 \le C_{31}s\|e^{k+1}\|_{\mathring{H}^{-1}_{\text{per}}}^2 + \frac{\varepsilon^2}{8}s\|\Delta e^{k+1}\|^2. \tag{3.32}$$

Similarly, the term I_8 is also decomposed into two parts: $I_8 = I_{8,1} + I_{8,2}$, with

$$I_{8,1} = -8As\left((\nabla(\Phi^{k+1} + \phi^{k+1}) \cdot \nabla e^{k+1})\nabla\Phi^{k+1}, \nabla e^{k+1}\right),$$

$$I_{8,2} = -8As\left(|\nabla\phi^{k+1}|^2\nabla e^{k+1}, \nabla e^{k+1}\right) = -8As\int_\Omega |\nabla e^{k+1}|^4 d\mathbf{x} \le 0.$$

For the first part $I_{8,1}$, the following estimate is available, in a similar way as (3.30)–(3.31):

$$I_{8,1} \le C_{32}s(\|\nabla\Phi^{k+1}\|_{L^6} + \|\nabla\phi^{k+1}\|_{L^6}) \cdot \|\nabla\Phi^{k+1}\|_{L^6} \cdot \|\nabla e^{k+1}\|_{L^6} \cdot \|\nabla e^{k+1}\|$$

$$
\begin{aligned}
&\le C_{33}C_7^2 s\|\nabla e^{k+1}\|_{L^6}\cdot\|\nabla e^{k+1}\|\\
&\le C_{34}C_7^2 s\|\Delta e^{k+1}\|\cdot\|e^{k+1}\|_{\mathring{H}_{\mathrm{per}}^{-1}}^{1/3}\cdot\|\Delta e^{k+1}\|^{2/3}\\
&\le C_{35}C_7^2 s\|\Delta e^{k+1}\|^{5/3}\cdot\|e^{k+1}\|_{\mathring{H}_{\mathrm{per}}^{-1}}^{1/3}\le C_{36}s\|e^{k+1}\|_{\mathring{H}_{\mathrm{per}}^{-1}}^2+\frac{\varepsilon^2}{8}s\|\Delta e^{k+1}\|^2,
\end{aligned}
$$

in which the $W^{1,6}$ bound (3.6) for the exact and numerical solutions was recalled in the second step, the 3-D Sobolev embedding from H_{per}^2 into $W^{1,6}$ and the estimate (3.15) were used in the third step, and the Young inequality was applied at the last step. Then we arrive at

$$
I_8=I_{8,1}+I_{8,2}\le I_{8,1}\le C_{36}s\|e^{k+1}\|_{\mathring{H}_{\mathrm{per}}^{-1}}^2+\frac{\varepsilon^2}{8}s\|\Delta e^{k+1}\|^2. \tag{3.33}
$$

The term I_9 can be handled in the same way as I_8. We begin with a decomposition $I_9=I_{9,1}+I_{9,2}$, with

$$
\begin{aligned}
I_{9,1}&=8As\left((\nabla(\Phi^k+\phi^k)\cdot\nabla e^k)\nabla\Phi^k,\nabla e^{k+1}\right),\\
I_{9,2}&=8As\left(|\nabla\phi^{k+1}|^2\nabla e^k,\nabla e^{k+1}\right).
\end{aligned}
$$

The following estimates can be carried out:

$$
\begin{aligned}
I_{9,1}&\le C_{37}s\left(\|\nabla\Phi^k\|_{L^6}+\|\nabla\phi^k\|_{L^6}\right)\cdot\|\nabla\Phi^k\|_{L^6}\cdot\|\nabla e^k\|_{L^6}\cdot\|\nabla e^{k+1}\|\\
&\le C_{38}C_7^2 s\|\nabla e^k\|_{L^6}\cdot\|\nabla e^{k+1}\|\\
&\le C_{39}C_7^2 s\|\Delta e^k\|\cdot\|e^{k+1}\|_{\mathring{H}_{\mathrm{per}}^{-1}}^{1/3}\cdot\|\Delta e^{k+1}\|^{2/3}\\
&\le C_{40}s\|e^{k+1}\|_{\mathring{H}_{\mathrm{per}}^{-1}}^2+\frac{\varepsilon^2}{16}s(\|\Delta e^{k+1}\|^2+\|\Delta e^k\|^2),\\
I_{9,2}&\le C_{41}s\|\nabla\phi^{k+1}\|_{L^6}^2\cdot\|\nabla e^k\|_{L^6}\cdot\|\nabla e^{k+1}\|\le C_{42}C_7^2 s\|\nabla e^k\|_{L^6}\cdot\|e^{k+1}\|\\
&\le C_{43}C_7^2 s\|\Delta e^k\|\cdot\|e^{k+1}\|_{\mathring{H}_{\mathrm{per}}^{-1}}^{1/3}\cdot\|\Delta e^{k+1}\|^{2/3}\\
&\le C_{44}s\|e^{k+1}\|_{\mathring{H}_{\mathrm{per}}^{-1}}^2+\frac{\varepsilon^2}{16}s(\|\Delta e^{k+1}\|^2+\|\Delta e^k\|^2).
\end{aligned}
$$

Consequently, we get

$$
I_9=I_{9,1}+I_{9,2}\le C_{45}s\|e^{k+1}\|_{\mathring{H}_{\mathrm{per}}^{-1}}^2+\frac{\varepsilon^2}{8}s(\|\Delta e^{k+1}\|^2+\|\Delta e^k\|^2). \tag{3.34}
$$

Finally, a combination of (3.7), (3.10), (3.11), (3.12), (3.13), (3.18), (3.22), (3.26), (3.32), (3.33) and (3.34) yields that

$$
\begin{aligned}
&\|e^{k+1}\|_{\mathring{H}_{\mathrm{per}}^{-1}}^2-\|e^k\|_{\mathring{H}_{\mathrm{per}}^{-1}}^2+2(\varepsilon^{-2}+\eta)s\|e^{k+1}\|^2+\frac{9}{8}\varepsilon^2 s\|\Delta e^{k+1}\|^2\\
&\quad\le C_{46}s\left(\|e^{k+1}\|_{\mathring{H}_{\mathrm{per}}^{-1}}^2+\|e^k\|_{\mathring{H}_{\mathrm{per}}^{-1}}^2\right)+\frac{3}{8}\varepsilon^2 s\|\Delta e^k\|^2+s\|\tau^k\|^2.
\end{aligned} \tag{3.35}
$$

Subsequently, an application of discrete Gronwall inequality leads to an $\ell^\infty(0, T; \mathring{H}^{-1}_{\text{per}}) \cap \ell^2(0, T; H^2_{\text{per}})$ convergence of the numerical scheme (2.15):

$$\|e^k\|^2_{\mathring{H}^{-1}_{\text{per}}} + \frac{3}{4}\varepsilon^2 s \sum_{l=0}^{k} \|\Delta e^l\|^2 \le C s^2, \tag{3.36}$$

for any $1 \le k \le K$. Note that the constant C depends on the exact solution, the physical parameter ε, and final time T, independent on s. The proof of Theorem 3.1 is finished.

Remark 3.2 The convergence constant appearing in (3.2) (in Theorem 3.1) is independent of s, while it does depend on the final time T and on the physical parameter ε. A detailed calculation reveals it is of the order $\exp\left(\varepsilon^{-k} T\right)$ (k is some integer), which comes from the application of the discrete Gronwall inequality in the convergence analysis.

There have been existing works on the improved convergence constant for the pure Cahn–Hilliard equation. Specifically, Feng and Prohl [32] proved—for a first-order in time, fully discrete finite element scheme—that the convergence constant is of order $O(e^{C_0 T} \varepsilon^{-m_0})$, for some positive integer m_0 and a constant C_0 independent of ε, instead of the singularly ε-dependent exponential growth. Similar estimates have also been obtained for the first order convex splitting scheme applied to the Allen–Cahn and Cahn–Hilliard equations in [30,31], respectively. In fact, these results give the sharpest convergence constant for the Cahn–Hilliard flow in the existing literature.

Such an elegant improvement was based on a subtle spectrum analysis for the linearized Cahn–Hilliard operator, provided in earlier publications [1,2,15–17]. On the other hand, such a linearized spectrum estimate is not (yet) available for FCH equation (1.5), due to the highly nonlinear nature of the expansion. In turn, an improvement of the convergence constant reported in (3.2) cannot be applied straightforwardly. This issue will be explored in the future works.

4 Finite Difference Spatial Discretization in 2D

4.1 Notation

In this subsection we define the discrete spatial difference operators, function space, inner products and norms, following the notations used in [28,50,53]. Let $\Omega = (0, L_x) \times (0, L_y)$, where, for simplicity, we assume $L_x = L_y =: L > 0$. We write $L = m \cdot h$, where m is a positive integer. The parameter $h = \frac{L}{m}$ is called the mesh or grid spacing. We define the following two uniform, infinite grids with grid spacing $h > 0$:

$$E := \{x_{i+1/2} \mid i \in \mathbb{Z}\}, \quad C := \{x_i \mid i \in \mathbb{Z}\},$$

where $x_i = x(i) := (i - 1/2) \cdot h$. Consider the following 2D discrete periodic function spaces:

$$\begin{aligned}
\mathcal{V}_{\text{per}} &:= \left\{ v : E \times E \to \mathbb{R} \mid v_{i+\frac{1}{2}, j+\frac{1}{2}} = v_{i+\frac{1}{2}+\alpha m, j+\frac{1}{2}+\beta m},\ \forall\, i, j, \alpha, \beta \in \mathbb{Z} \right\}, \\
\mathcal{C}_{\text{per}} &:= \left\{ v : C \times C \to \mathbb{R} \mid v_{i,j} = v_{i+\alpha m, j+\beta m},\ \forall\, i, j, \alpha, \beta \in \mathbb{Z} \right\}, \\
\mathcal{E}^{\text{ew}}_{\text{per}} &:= \left\{ v : E \times C \to \mathbb{R} \mid v_{i+\frac{1}{2}, j} = v_{i+\frac{1}{2}+\alpha m, j+\beta m},\ \forall\, i, j, \alpha, \beta \in \mathbb{Z} \right\}, \\
\mathcal{E}^{\text{ns}}_{\text{per}} &:= \left\{ v : C \times E \to \mathbb{R} \mid v_{i, j+\frac{1}{2}} = v_{i+\alpha m, j+\frac{1}{2}+\beta m},\ \forall\, i, j, \alpha, \beta \in \mathbb{Z} \right\}.
\end{aligned}$$

The functions of $\mathcal{V}_{\text{per}}$ are called *vertex centered functions*; those of $\mathcal{C}_{\text{per}}$ are called *cell centered functions*. The functions of $\mathcal{E}^{\text{ew}}_{\text{per}}$ are called *east-west edge-centered functions*, and the functions of $\mathcal{E}^{\text{ns}}_{\text{per}}$ are called *north-south edge-centered functions*. We also define the mean zero space

$$\mathring{\mathcal{C}}_{\text{per}} := \left\{ \nu \in \mathcal{C}_{\text{per}} \,|\overline{\nu} := \frac{h^2}{|\Omega|} \sum_{i,j=1}^{m} \nu_{i,j} = 0 \right\}.$$

We now introduce the important difference and average operators on the spaces:

$$A_x \nu_{i+1/2,\square} := \frac{1}{2}\left(\nu_{i+1,\square} + \nu_{i,\square}\right), \quad D_x \nu_{i+1/2,\square} := \frac{1}{h}\left(\nu_{i+1,\square} - \nu_{i,\square}\right),$$
$$A_y \nu_{\square,i+1/2} := \frac{1}{2}\left(\nu_{\square,i+1} + \nu_{\square,i}\right), \quad D_y \nu_{\square,i+1/2} := \frac{1}{h}\left(\nu_{\square,i+1} - \nu_{\square,i}\right),$$

with $A_x,\ D_x : \mathcal{C}_{\text{per}} \to \mathcal{E}^{\text{ew}}_{\text{per}}$ if $\square$ is an integer, and $A_x,\ D_x : \mathcal{E}^{\text{ns}}_{\text{per}} \to \mathcal{V}_{\text{per}}$ if $\square$ is a half-integer, with $A_y,\ D_y : \mathcal{C}_{\text{per}} \to \mathcal{E}^{\text{ns}}_{\text{per}}$ if $\square$ is an integer, and $A_y,\ D_y : \mathcal{E}^{\text{ew}}_{\text{per}} \to \mathcal{V}_{\text{per}}$ if $\square$ is a half-integer. Likewise,

$$a_x \nu_{i,\square} := \frac{1}{2}\left(\nu_{i+1/2,\square} + \nu_{i-1/2,\square}\right), \quad d_x \nu_{i,\square} := \frac{1}{h}\left(\nu_{i+1/2,\square} - \nu_{i-1/2,\square}\right),$$
$$a_y \nu_{\square,j} := \frac{1}{2}\left(\nu_{\square,j+1/2} + \nu_{\square,j-1/2}\right), \quad d_y \nu_{\square,j} := \frac{1}{h}\left(\nu_{\square,j+1/2} - \nu_{\square,j-1/2}\right),$$

with $a_x,\ d_x : \mathcal{E}^{\text{ew}}_{\text{per}} \to \mathcal{C}_{\text{per}}$ if $\square$ is an integer, and $a_x,\ d_x : \mathcal{V}_{\text{per}} \to \mathcal{E}^{\text{ns}}_{\text{per}}$ if $\square$ is a half-integer; and with $a_y,\ d_y : \mathcal{E}^{\text{ns}}_{\text{per}} \to \mathcal{C}_{\text{per}}$ if $\square$ is an integer, and $a_y,\ d_y : \mathcal{V}_{\text{per}} \to \mathcal{E}^{\text{ew}}_{\text{per}}$ if $\square$ is a half-integer.

Define the 2D center-to-vertex derivatives $\mathfrak{D}_x,\ \mathfrak{D}_y : \mathcal{C}_{\text{per}} \to \mathcal{V}_{\text{per}}$ component-wise as

$$\begin{aligned}
\mathfrak{D}_x \nu_{i+1/2,j+1/2} &:= A_y(D_x\nu)_{i+1/2,j+1/2} = D_x(A_y\nu)_{i+1/2,j+1/2} \\
&= \frac{1}{2h}\left(\nu_{i+1,j+1} - \nu_{i,j+1} + \nu_{i+1,j} - \nu_{i,j}\right), \\
\mathfrak{D}_y \nu_{i+1/2,j+1/2} &:= A_x(D_y\nu)_{i+1/2,j+1/2} = D_y(A_x\nu)_{i+1/2,j+1/2} \\
&= \frac{1}{2h}\left(\nu_{i+1,j+1} - \nu_{i+1,j} + \nu_{i,j+1} - \nu_{i,j}\right).
\end{aligned}$$

The utility of these definitions is that the differences $\mathfrak{D}_x$ and $\mathfrak{D}_y$ are collocated on the grid, unlike the case for D_x, D_y. Define the 2D vertex-to-center derivatives $\mathfrak{d}_x,\ \mathfrak{d}_y : \mathcal{V}_{\text{per}} \to \mathcal{C}_{\text{per}}$ component-wise as

$$\begin{aligned}
\mathfrak{d}_x \nu_{i,j} &:= a_y(d_x\nu)_{i,j} = d_x(a_y\nu)_{i,j} \\
&= \frac{1}{2h}\left(\nu_{i+1/2,j+1/2} - \nu_{i-1/2,j+1/2} + \nu_{i+1/2,j-1/2} - \nu_{i-1/2,j-1/2}\right), \\
\mathfrak{d}_y \nu_{i,j} &:= a_x(d_y\nu)_{i,j} = d_y(a_x\nu)_{i,j} \\
&= \frac{1}{2h}\left(\nu_{i+1/2,j+1/2} - \nu_{i+1/2,j-1/2} + \nu_{i-1/2,j+1/2} - \nu_{i-1/2,j-1/2}\right).
\end{aligned}$$

Now the discrete gradient operator, ∇_h^v: $\mathcal{C}_{\text{per}} \to \mathcal{V}_{\text{per}} \times \mathcal{V}_{\text{per}}$, becomes

$$\nabla_h^v \nu_{i+1/2,j+1/2} := (\mathfrak{D}_x \nu_{i+1/2,j+1/2}, \mathfrak{D}_y \nu_{i+1/2,j+1/2}).$$

The standard 2D discrete Laplacian, $\Delta_h : \mathcal{C}_{\text{per}} \to \mathcal{C}_{\text{per}}$, is given by

$$\Delta_h \nu_{i,j} := d_x(D_x\nu)_{i,j} + d_y(D_y\nu)_{i,j} = \frac{1}{h^2}\left(\nu_{i+1,j} + \nu_{i-1,j} + \nu_{i,j+1} + \nu_{i,j-1} - 4\nu_{i,j}\right).$$

The 2D vertex-to-center average, $\mathfrak{A} : \mathcal{V}_{\text{per}} \to \mathcal{C}_{\text{per}}$, is defined to be

$$\mathfrak{A}v_{i,j} := \frac{1}{4}\left(v_{i-1/2,j-1/2} + v_{i-1/2,j+1/2} + v_{i+1/2,j+1/2} + v_{i+1/2,j-1/2}\right),$$

and the 2D center-to-vertex average, $\mathfrak{a} : \mathcal{C}_{\text{per}} \to \mathcal{V}_{\text{per}}$, becomes

$$\mathfrak{a}v_{i+1/2,j+1/2} := \frac{1}{4}\left(v_{i,j} + v_{i+1,j} + v_{i,j+1} + v_{i+1,j+1}\right).$$

The 2D *skew* Laplacian, $\Delta_h^v : \mathcal{C}_{\text{per}} \to \mathcal{C}_{\text{per}}$, is introduced as

$$\Delta_h^v v_{i,j} = \mathfrak{d}_x(\mathfrak{D}_x v)_{i,j} + \mathfrak{d}_y(\mathfrak{D}_y v)_{i,j} = \frac{1}{2h^2}\left(v_{i+1,j+1} + v_{i-1,j+1} + v_{i+1,j-1} + v_{i-1,j-1} - 4v_{i,j}\right).$$

In addition, the 2D undivided laplacian operator for non-constant mobility is

$$\nabla_h^v \cdot \left(\mathcal{M}^v(v)\nabla_h^v v\right)_{ij} := \mathfrak{d}_x(\mathcal{M}^v(v)\,\mathfrak{D}_x v)_{i,j} + \mathfrak{d}_y(\mathcal{M}^v(v)\,\mathfrak{D}_y v)_{i,j}, \quad \mathcal{M}^v(v) = (\mathfrak{a}\mathcal{M}(v))_{i+1/2,j+1/2}$$

Hence, the 2D discrete p-Laplacian operator turns out to be

$$\nabla_h^v \cdot \left(\left|\nabla_h^v v\right|^{p-2}\nabla_h^v v\right)_{ij} := \mathfrak{d}_x(r\,\mathfrak{D}_x v)_{i,j} + \mathfrak{d}_y(r\,\mathfrak{D}_y v)_{i,j},$$

with

$$r_{i+\frac{1}{2},j+\frac{1}{2}} := \left[(\mathfrak{D}_x u)^2_{i+\frac{1}{2},j+\frac{1}{2}} + (\mathfrak{D}_y u)^2_{i+\frac{1}{2},j+\frac{1}{2}}\right]^{\frac{p-2}{2}}.$$

Clearly, for $p = 2$, we have $\Delta_h^v v = \nabla_h^v \cdot \left(\left|\nabla_h^v v\right|^{p-2}\nabla_h^v v\right)$.

Now we are ready to define the following grid inner products:

$$(v,\xi)_2 := h^2\sum_{i=1}^m\sum_{j=1}^n v_{i,j}\psi_{i,j}, \quad v,\xi \in \mathcal{C}_{\text{per}}, \qquad \langle v,\xi\rangle := (\mathfrak{A}(v\xi),1)_2, \quad v,\xi \in \mathcal{V}_{\text{per}},$$
$$[v,\xi]_{\text{ew}} := (A_x(v\xi),1)_2, \quad v,\xi \in \mathcal{E}^{\text{ew}}_{\text{per}}, \qquad [v,\xi]_{\text{ns}} := \left(A_y(v\xi),1\right)_2, \quad v,\xi \in \mathcal{E}^{\text{ns}}_{\text{per}}.$$

Suppose that $\zeta \in \mathring{\mathcal{C}}_{\text{per}}$, then there is a unique solution $\mathsf{T}_h[\zeta] \in \mathring{\mathcal{C}}_{\text{per}}$ such that $-\Delta_h \mathsf{T}_h[\zeta] = \zeta$. We often write, in this case, $\mathsf{T}_h[\zeta] = -\Delta_h^{-1}\zeta$. The discrete analog of the $\mathring{H}^{-1}_{\text{per}}$ inner product is defined as

$$(\zeta,\xi)_{-1} := (\zeta, \mathsf{T}_h[\xi])_2 = (\mathsf{T}_h[\zeta],\xi)_2, \quad \zeta,\xi \in \mathring{\mathcal{C}}_{\text{per}}.$$

where summation-by-parts formulae [21,53] guarantees the symmetry and the second equality.

We now define the following norms for cell-centered functions. If $v \in \mathring{\mathcal{C}}_{\text{per}}$, then $\|v\|^2_{-1} = (v,v)_{-1}$. If $v \in \mathcal{C}_{\text{per}}$, then $\|v\|_2^2 := (v,v)_2$; $\|v\|_p^p := (|v|^p,1)_2$ $(1 \le p < \infty)$, and $\|v\|_\infty := \max_{\substack{1\le i\le m\\ 1\le j\le n}} \left|v_{i,j}\right|$. Similarly, we define the gradient norms: for $v \in \mathcal{C}_{\text{per}}$,

$$\left\|\nabla_h^v v\right\|_p^p := \langle|\nabla_h^v v|^p, 1\rangle, \quad |\nabla_h^v v|^p := \left[(\mathfrak{D}_x v)^2 + (\mathfrak{D}_y v)^2\right]^{\frac{p}{2}} = \left[\nabla_h^v v \cdot \nabla_h^v v\right]^{\frac{p}{2}} \in \mathcal{V}_{\text{per}}, \quad 2 \le p < \infty,$$

and

$$\|\nabla_h v\|_2^2 := [D_x v, D_x v]_{\text{ew}} + \left[D_y v, D_y v\right]_{\text{ns}}.$$

4.2 Fully Discrete Finite Difference Scheme

With the machinery in last subsection, the discrete energy of FCH can be rewritten as:

$$\mathcal{F}_h(\phi) = \mathcal{F}_{c,h}(\phi) - \mathcal{F}_{e,h}(\phi) \tag{4.1}$$

where

$$\mathcal{F}_{c,h}(\phi) = \frac{\varepsilon^{-2}}{2}\|\phi\|_6^6 + \left(\frac{\varepsilon^{-2}}{2} + \frac{\eta}{2}\right)\|\phi\|_2^2 + \frac{\varepsilon^2}{2}\|\Delta_h\phi\|_2^2 + \mathcal{H}_h(\phi), \tag{4.2}$$

$$\mathcal{F}_{e,h}(\phi) = \left(\varepsilon^{-2} + \frac{\eta}{4}\right)\|\phi\|_4^4 + \left(1 + \frac{\eta\varepsilon^2}{2}\right)\left\|\nabla_h^v\phi\right\|_2^2 + A\|\phi\|_4^4 + A\left\|\nabla_h^v\phi\right\|_4^4, \tag{4.3}$$

and

$$\mathcal{H}_h(\phi) = A\|\phi\|_4^4 + A\left\|\nabla_h^v\phi\right\|_4^4 + 3\left(\phi^2, \mathfrak{A}(\left|\nabla_h^v\phi\right|^2)\right)_2. \tag{4.4}$$

Proposition 4.1 *Suppose $\phi \in \mathcal{C}_{\text{per}}$. The first variational derivative of $\mathcal{H}_h(\phi)$ is*

$$\begin{aligned}\delta\mathcal{H}_h(\phi) = {} & 4A\phi^3 - 4A\left(\mathfrak{d}_x\left[(\mathfrak{D}_x\phi)^2 + (\mathfrak{D}_y\phi)^2\right]\mathfrak{D}_x\phi\right) + \mathfrak{d}_y\left(\left[(\mathfrak{D}_x\phi)^2 + (\mathfrak{D}_y\phi)^2\right]\mathfrak{D}_y\phi\right)\Big) \\ & + 6\phi\mathfrak{A}[(\mathfrak{D}_x\phi)^2 + (\mathfrak{D}_y\phi)^2] - 6\left(\mathfrak{d}_x\left(\mathfrak{a}\left(\phi^2\right)\mathfrak{D}_x\phi\right) + \mathfrak{d}_y\left(\mathfrak{a}\left(\phi^2\right)\mathfrak{D}_y\phi\right)\right).\end{aligned}$$

The following estimate is needed in the convexity analysis for $\mathcal{H}_h(\phi)$.

Lemma 4.2 *For $f \in \mathcal{V}_{\text{per}}$, we have*

$$\langle 1, f^2\rangle \geq \left(1, (\mathfrak{A}f)^2\right)_2. \tag{4.5}$$

Proof Based on the definition of the average operator $\mathfrak{A}$, we have the following expansion and estimate:

$$\begin{aligned}(\mathfrak{A}f)_{i,j}^2 &= \left(\frac{1}{4}(f_{i-1/2,j-1/2} + f_{i+1/2,j-11/2} + f_{i-1/2,j+1/2} + f_{i+1/2,j+1/2})\right)^2 \\ &\leq \frac{1}{4}\left(f_{i-1/2,j-1/2}^2 + f_{i+1/2,j-1/2}^2 + f_{i-1/2,j+1/2}^2 + f_{i+1/2,j+1/2}^2\right).\end{aligned} \tag{4.6}$$

Therefore, by summing over the grid index, in combination with the index counting, we arrive at

$$\sum_{i,j}(\mathfrak{A}f)_{i,j}^2 \leq \sum_{i,j} f_{i+1/2,j+1/2}^2. \tag{4.7}$$

In turn, estimate (4.5) is a direct consequence of this inequality. This finishes the proof of this lemma. □

Subsequently, the convexity of $\mathcal{H}_h(\phi)$, $\mathcal{F}_{c,h}(\phi)$ and $\mathcal{F}_{e,h}(\phi)$ are stated below.

Lemma 4.3 *Suppose that $\phi \in \mathcal{C}_{\text{per}}$ and $A \geq 1$ then $\mathcal{H}_h(\phi)$, $\mathcal{F}_{c,h}(\phi)$ and $\mathcal{F}_{e,h}(\phi)$ are strictly convex.*

Proof We denote $g(\phi) := 3\phi^2\mathcal{A}\left|\nabla_h^v\phi\right|^2 \in \mathcal{C}_{\text{per}}$. Consequently, we obtain $\mathcal{G}_h[\phi] = (1, g(\phi))_2$ and $\mathcal{H}_h[\phi] = \mathcal{G}_h[\phi] + A(\|\phi\|_4^4 + \left\|\nabla_h^v\phi\right\|_4^4)$. The following inequalities are evaluated at a point-wise level, for any ϕ_1, ϕ_2:

$$\left(\frac{\phi_1+\phi_2}{2}\right)^2 \le \frac{\phi_1^2+\phi_2^2}{2}, \quad \text{at } (i,j),$$
$$\left|\nabla_h^v\left(\frac{\phi_1+\phi_2}{2}\right)\right|^2 \le \frac{|\nabla_h^v\phi_1|^2+|\nabla_h^v\phi_2|^2}{2}, \quad \text{at } (i+1/2, j+1/2),$$

which come from the convexity of $q_2(x) = x^2$ and $r_2(\boldsymbol{x}) = \boldsymbol{x}\cdot\boldsymbol{x}$. Moreover, taking an average operator $\mathfrak{A}$ to the second inequality leads to the following estimate:

$$\mathfrak{A}\left(\left|\nabla_h^v\left(\frac{\phi_1+\phi_2}{2}\right)\right|^2\right) \le \frac{\mathfrak{A}(|\nabla_h^v\phi_1|^2)+\mathfrak{A}(|\nabla_h^v\phi_2|^2)}{2}, \quad \text{at } (i,j).$$

These inequalities in turn imply that

$$g\left(\frac{\phi_1+\phi_2}{2}\right) = 3\left(\frac{\phi_1+\phi_2}{2}\right)^2\cdot\mathfrak{A}\left(\left|\nabla_h^v\left(\frac{\phi_1+\phi_2}{2}\right)\right|^2\right) \le 3\frac{\phi_1^2+\phi_2^2}{2}\cdot\frac{\mathfrak{A}(|\nabla_h^v\phi_1|^2)+\mathfrak{A}(|\nabla_h^v\phi_2|^2)}{2},$$

at a point-wise level. A careful comparison with $\frac{g(\phi_1)+g(\phi_2)}{2} = \frac{3\phi_1^2|\nabla_h^v\phi_1|^2+3\phi_2^2|\nabla_h^v\phi_2|^2}{2}$ shows that

$$\begin{aligned}\frac{g(\phi_1)+g(\phi_2)}{2} - g\left(\frac{\phi_1+\phi_2}{2}\right) &\ge \frac{3(\phi_1^2-\phi_2^2)(\mathfrak{A}(|\nabla_h^v\phi_1|^2)-\mathfrak{A}(|\nabla_h^v\phi_2|^2))}{4}\\ &\ge -\frac{3}{8}\left((\phi_1^2-\phi_2^2)^2+(\mathfrak{A}(|\nabla_h^v\phi_1|^2-|\nabla_h^v\phi_2|^2))^2\right).\end{aligned} \tag{4.8}$$

Similarly, the convexity of $q_4(x) = x^4$ and $r_4(\boldsymbol{x}) = |\boldsymbol{x}|^4$ indicates the following inequalities:

$$\frac{\phi_1^4+\phi_2^4}{2} - \left(\frac{\phi_1+\phi_2}{2}\right)^4 \ge \frac{3}{8}\left(\phi_1^4+\phi_2^4-2\phi_1^2\phi_2^2\right) = \frac{3}{8}\left(\phi_1^2-\phi_2^2\right)^2, \quad \text{at } (i,j), \tag{4.9}$$

and

$$\begin{aligned}&\frac{|\nabla_h^v\phi_1|^4+|\nabla_h^v\phi_2|^4}{2} - \left|\nabla_h^v\left(\frac{\phi_1+\phi_2}{2}\right)\right|^4 \ge \frac{3}{8}\left(|\nabla_h^v\phi_1|^4+|\nabla_h^v\phi_2|^4-2|\nabla_h^v\phi_1|^2\cdot|\nabla_h^v\phi_2|^2\right)\\ \ge\ &\frac{3}{8}\left(|\nabla_h^v\phi_1|^2-|\nabla_h^v\phi_2|^2\right)^2, \quad \text{at } (i+1/2, j+1/2).\end{aligned} \tag{4.10}$$

Meanwhile, the following estimate is available, with an application of inequality (4.5) in Lemma 4.2, by taking $f = |\nabla_h^v\phi_1|^2-|\nabla_h^v\phi_2|^2$:

$$\langle 1, (|\nabla_h^v\phi_1|^2-|\nabla_h^v\phi_2|^2)^2\rangle \ge \left(1, \mathfrak{A}(|\nabla_h^v\phi_1|^2-|\nabla_h^v\phi_2|^2))^2\right)_2. \tag{4.11}$$

As a result, a combination of (4.8), (4.9), (4.10) and (4.11) yields

$$\frac{\mathcal{H}_h(\phi_1)+H(\phi_2)}{2} - \mathcal{H}_h\left(\frac{\phi_1+\phi_2}{2}\right) \ge 0, \quad \forall\phi_1,\ \phi_2, \quad \text{if } A \ge 1.$$

The convexity of $\mathcal{H}_h$ is assured under the condition $A \ge 1$.

The convexity property of $\mathcal{F}_{c,h}(\phi)$ and $\mathcal{F}_{e,h}(\phi)$ follows from the convexity of $\mathcal{H}_h(\phi)$.

□

According to Proposition 4.1 and some other standard calculations [46], the fully discretized finite difference scheme can be rewritten as: given $f, g \in \mathcal{C}_{\text{per}}$, find $\phi^{k+1}, \tilde{\mu}^{k+1} \in \mathcal{C}_{\text{per}}$ such that

$$\phi^{k+1} - s\Delta_h \tilde{\mu}^{k+1} = g, \tag{4.12}$$

where

$$\begin{aligned} \tilde{\mu}^{k+1} &= \delta_\phi \mathcal{F}_{c,h}(\phi^{k+1}) - \delta_\phi \mathcal{F}_{e,h}(\phi^k) \\ &= 3\varepsilon^{-2}(\phi^{k+1})^5 + 4A(\phi^{k+1})^3 + (\varepsilon^{-2} + \eta)\phi^{k+1} + 6(\phi^{k+1})^2 \mathfrak{A}(|\nabla_h^v \phi^{k+1}|^2) + \varepsilon^2 \Delta_h^2 \phi^{k+1} \\ &\quad - 6\nabla_h^v \cdot \left(\mathfrak{a}\left((\phi^{k+1})^2\right)\nabla_h^v \phi^{k+1}\right) - 4A\nabla_h^v \cdot (|\nabla_h^v \phi^{k+1}|^2 \nabla_h^v \phi^{k+1}) + f, \end{aligned} \tag{4.13}$$

with

$$g := \phi^k, \ \ f := -(4\varepsilon^{-2} + \eta)(\phi^k)^3 + (2 + \eta\varepsilon^2)\Delta_h^v \phi^k - 4A(\phi^k)^3 + 4A\nabla_h^v \cdot (|\nabla_h^v \phi^k|^2 \nabla_h^v \phi^k). \tag{4.14}$$

This scheme is mass-conservative in the sense that $\phi - g \in \mathring{\mathcal{C}}_{\text{per}}$.

Theorem 4.4 *The fully discrete scheme* (4.12)–(4.14) *is unconditionally discrete energy stable,* $\mathcal{F}_h(\phi^{k+1}) \le \mathcal{F}_h(\phi^k)$*, and unconditionally uniquely solvable.*

Proof The proof follows from Lemma 4.3 and the discrete version of (2.4) found in [53]. □

The following lemma, excerpted as Proposition 2.2 in a recent work [29], plays an important role to derive a uniform bound for the numerical solution in the discrete L^∞, $W^{1,6}$ and H^2 norms.

Lemma 4.5 [29] *For any* $\phi \in \mathcal{C}_{\text{per}}$ *with* $\overline{\phi} = 0$*, we have*

$$\|\Delta_h \phi\|_2^2 \ge C\|\phi\|_{H_h^2}^2, \quad \text{with } \|\phi\|_{H_h^2}^2 := \|\phi\|_2^2 + \|\nabla_h \phi\|_2^2 + \|\Delta_h \phi\|_2^2, \tag{4.15}$$

$$\|\phi\|_\infty \le C\|\phi\|_{H_h^2}, \tag{4.16}$$

$$\|\phi\|_{W_h^{1,6}} := \|\phi\|_6 + \|\nabla_h^v \phi\|_6 \le C\|\phi\|_{H_h^2}, \tag{4.17}$$

with C *only dependent on* Ω.

Following similar ideas as in the analyses for the semi-discrete case, we are able to obtain the following bound, analogous to (3.6)

$$\|\Phi^k\|_\infty, \ \|\Phi^k\|_{W_h^{1,6}}, \ \|\Phi^k\|_{H_h^2} \le C, \quad \|\phi^k\|_\infty, \ \|\phi^k\|_{W_h^{1,6}}, \ \|\phi^k\|_{H_h^2} \le C, \tag{4.18}$$

for any $k \ge 0$. And also, the $\ell^\infty(0, T; H^{-1}) \cap \ell^2(0, T; H^2)$ convergence for the fully discrete scheme (4.12)–(4.14) could be derived. The detailed proofs are skipped for the sake of brevity and are left to interested readers.

For the convergence theorem, we define the regularity class

$$\mathcal{R}_2 := C^2([0, T]; C_{\text{per}}^0(\Omega)) \cap C^1([0, T]; C_{\text{per}}^4(\Omega)) \cap L^\infty([0, T]; C_{\text{per}}^8(\Omega)). \tag{4.19}$$

We have the following error estimate.

Theorem 4.6 *Let $\Phi \in \mathcal{R}_2$ (see (4.19)) be the exact periodic solution of the FCH equation (1.5) with the initial data $\Phi(0) = \phi_0 \in H^2_{\text{per}}(\Omega)$. Suppose ϕ is the fully-discrete solution of (4.12)–(4.14). Then the following convergence result holds as s, h goes to zero:*

$$\|\Phi(t_k) - \phi^k\|_{-1} + \left(\varepsilon^2 s \sum_{\ell=0}^{k} \|\Delta_h(\Phi(t_\ell) - \phi^\ell)\|^2 \right)^{1/2} \le C(s + h^2), \tag{4.20}$$

where the constant $C > 0$ is independent of s and h.

Remark 4.7 There have been extensive works of energy stable finite difference schemes for various gradient flows in the existing literature. On the other hand, it is the first time in this article to analyze the skew-symmetric finite difference operators in an H^{-1} gradient flow, with a detailed convergence estimate established. In particular, the proof of Lemma 4.3 is not a direct extension of that for Lemma 2.2, due to the complicated skew-symmetric and average operators involved in the analysis, which come from the highly nonlinear 4-Laplacian terms in an H^{-1} format. These techniques are expected to be applicable to many other nonlinear H^{-1} gradient flows involved with p-Laplacian terms.

5 Preconditioned Steepest Descent (PSD) Solver

In this section we describe a preconditioned steepest descent (PSD) algorithm for advancing the convex–concave decomposition scheme in time following the practical and theoretical framework in [28]. The fully discrete scheme (4.12)–(4.14) can be recast as a minimization problem with an energy that involves the $\|\cdot\|_{-1}^2$ norm: For any $\phi \in \mathcal{C}_{\text{per}}$,

$$\begin{aligned} E_h[\phi] = {} & \frac{1}{2}\|\phi - g\|_{-1}^2 + \frac{s\varepsilon^{-2}}{2}\|\phi\|_6^6 + \frac{s(\varepsilon^{-2}+\eta)}{2}\|\phi\|_2^2 \\ & + As\|\phi\|_4^4 + As\left\|\nabla_h^v u\right\|_4^4 + 3\left(\phi^2, \mathfrak{A}\left(|\nabla_h^v \phi|^2\right)\right)_2 + \frac{s\varepsilon^2}{2}\|\Delta_h \phi\|_2^2 + s(g, \phi), \end{aligned} \tag{5.1}$$

which is strictly convex provided that $A \ge 1$. One will observe that the fully discrete scheme (4.12)–(4.14) is the discrete variation of the strictly convex energy (5.1) set equal to zero. The nonlinear scheme at a fixed time level may be expressed as

$$\mathcal{N}_h[\phi] = f, \tag{5.2}$$

where

$$\begin{aligned} \mathcal{N}_h[\phi] = {} & -\Delta_h^{-1}(\phi - g) + 3s\varepsilon^{-2}\phi^5 + 4sA\phi^3 + s(\varepsilon^{-2}+\eta)\phi + 6s\phi^2\mathfrak{A}(|\nabla_h^v\phi|^2) \\ & -6s\nabla_h^v \cdot \left(\mathfrak{a}\left(\phi^2\right)\nabla_h^v\phi\right) - 4sA\nabla_h^v \cdot (|\nabla_h^v\phi|^2\nabla_h^v\phi) + s\varepsilon^2\Delta_h^2\phi. \end{aligned} \tag{5.3}$$

The main idea of the PSD solver is to use a linearized version of the nonlinear operator as a pre-conditioner, or in other words, as a metric for choosing the search direction. A linearized version of the nonlinear operator $\mathcal{N}$ is defined as follows: $\mathcal{L}_h : \mathring{\mathcal{C}}_{\text{per}} \to \mathring{\mathcal{C}}_{\text{per}}$,

$$\mathcal{L}_h[\psi] := -\Delta_h^{-1}\psi + s(4\varepsilon^{-2} + \eta + 4A + 6)\psi - s(6 + 4A)\Delta_h\psi + s\varepsilon^2\Delta_h^2\psi.$$

Clearly, this is a positive, symmetric operator, and we use this as a pre-conditioner for the method. Specifically, this "metric" is used to find an appropriate search direcction for our

steepest descent solver [28]. Given the current iterate $\phi^n \in \mathcal{C}_{\text{per}}$, we define the following *search direction* problem: find $d^n \in \mathring{\mathcal{C}}^3_{\text{per}}$ such that

$$\mathcal{L}_h[d^n] = f - \mathcal{N}_h[\phi^n] := r^n,$$

where r^n is the nonlinear residual of the nth iterate ϕ^n. This last equation can be solved efficiently using the Fast Fourier Transform (FFT).

We then define the next iterate as

$$\phi^{n+1} = \phi^n + \overline{\alpha} d^n, \tag{5.4}$$

where $\overline{\alpha} \in \mathbb{R}$ is the unique solution to the steepest descent line minimization problem

$$\overline{\alpha} := \underset{\alpha \in \mathbb{R}}{\text{argmax}}\, E_h[\phi^n + \alpha d^n] = \underset{\alpha \in \mathbb{R}}{\text{argzero}}\, \delta E_h[\phi^n + \alpha d^n](d^n). \tag{5.5}$$

The theory in [28] suggests that $\phi^n \to \phi^{k+1}$ geometrically as $n \to \infty$, where $\mathcal{N}_h[\phi^{k+1}] = f$, i.e., ϕ^{k+1} is the solution of the scheme (4.12)–(4.14) at time level $k+1$. Furthermore, the convergence rate is independent of h.

In particular, it is observed that, although the proposed numerical scheme (4.12)–(4.14) is highly nonlinear (due to the implicit treatment of the nonlinear terms), the PSD solver is adequate for solving such a system, since the unique solvability has been guaranteed by Theorem 2.5.

6 Numerical Results

We perform some numerical experiments with the PSD solver to support the theoretical results in previous sections. The finite difference search direction equations and Poisson equations are solved efficiently using the Fast Fourier Transform (FFT). Though we do not present it here, we can also implement the scheme by using the pseudo-spectral method for spatial discretization [8,18,28,38].

6.1 Convergence Test

In this numerical experiment, we apply the benchmark problem in [19,42] to show that our scheme is first order accurate in time. The convergence test is performed with the initial data given by

$$\begin{aligned}\phi(x, y, 0) = 2\exp\left[\sin\left(\frac{2\pi x}{L_x}\right) + \sin\left(\frac{2\pi y}{L_y}\right) - 2\right] \\ +2.2\exp\left[-\sin\left(\frac{2\pi x}{L_x}\right) - \sin\left(\frac{2\pi y}{L_y}\right) - 2\right] - 1.\end{aligned} \tag{6.1}$$

We use a quadratic refinement path, i.e., $s = Ch^2$. At the final time $T = 0.32$, we expect the global error to be $\mathcal{O}(s) + \mathcal{O}(h^2) = \mathcal{O}(h^2)$ in either the ℓ^2 or ℓ^∞ norm, as $h, s \to 0$. Since an exact solution is not available, instead of calculating the error at the final time, we compute the Cauchy difference, which is defined as $\delta_\phi := \phi_{h_f} - \mathcal{I}_c^f(\phi_{h_c})$, where $\mathcal{I}_c^f$ is a bilinear interpolation operator. This requires having a relatively coarse solution, parametrized by h_c, and a relatively fine solution, parametrized by h_f, where $h_c = 2h_f$, at the same final time. The Cauchy difference is also expected to be $\mathcal{O}(s) + \mathcal{O}(h^2) = \mathcal{O}(h^2)$, as $h, s \to 0$. The other parameters are given by $L_x = L_y = 3.2$, $\varepsilon = 0.18$, $A = 1.0$, $\eta = 1.0$, $s = 0.1h^2$. The norms

Table 1 Errors, convergence rates, average iteration numbers and average CPU time (in seconds) for each time step. Parameters are given in the text, and the initial data is defined in (6.1). The refinement path is $s = 0.1h^2$

h_c	h_f	$\|\delta_\phi\|_2$	Rate	$\#_{iter}$	$T_{cpu}(h_f)$
$\frac{3.2}{16}$	$\frac{3.2}{32}$	1.8131×10^{-2}	–	27	0.0136
$\frac{3.2}{32}$	$\frac{3.2}{64}$	4.2725×10^{-3}	2.09	25	0.0493
$\frac{3.2}{64}$	$\frac{3.2}{128}$	7.7211×10^{-4}	2.47	19	0.1534
$\frac{3.2}{128}$	$\frac{3.2}{256}$	1.7075×10^{-4}	2.18	11	0.4809
$\frac{3.2}{256}$	$\frac{3.2}{512}$	4.0134×10^{-5}	2.09	05	2.1579

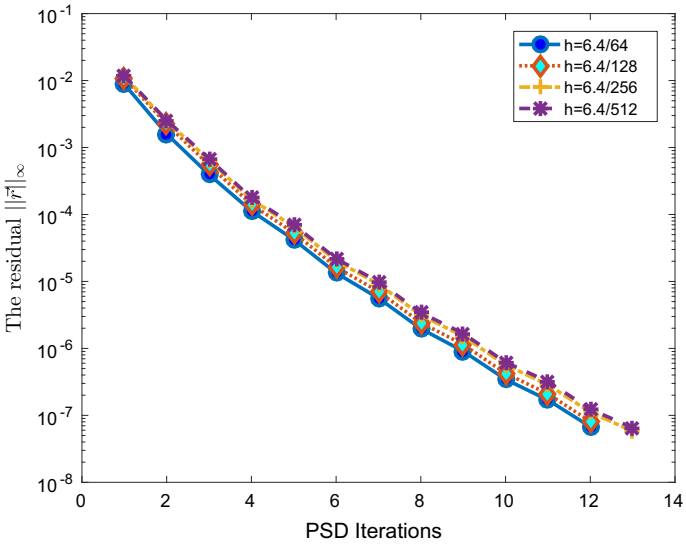

Fig. 1 Solver convergence (complexity) test for the problem defined in Sect. 6.1. The only difference is that for this test, we use a fixed time step size, $s = 1.0 \times 10^{-5}$ for all runs. We plot on a semi-log scale of the residual $\|r^n\|_\infty$ with respect to the PSD iteration count n at the 20th time step, i.e., $t = 2.0 \times 10^{-4}$. The initial data is defined in (6.1), $L_x = L_y = 6.4$, $\varepsilon = 0.18$, $A = 1.0$, $\eta = 1.0$, and the grid sizes are as specified in the legend. We observe that the residual is decreasing by a nearly constant factor for each iteration

of Cauchy difference, the convergence rates, average iteration number and average CPU time (in seconds) can be found in Table 1. The results confirm our expectation for the convergence order and also demonstrate the efficiency of our algorithm. Moreover, the semi-log scale of the residual $\|r^n\|_\infty$ with respect to the PSD iterations can be found in Fig. 1, which confirms the expected geometric convergence rate of the PSD solver predicted by the theory in [28].

6.2 Long Time Simulation of Benchmark Problem

Time snapshots of the benchmark problem in [19,42] for the long time test can be found in Fig. 2. The initial data is defined in (6.1) and the other parameters are given by $L_x = L_y = 6.4$, $\varepsilon = 0.18$, $A = 1.0$, $\eta = 1.0$, $s = 1 \times 10^{-4}$ and $h = 6.4/256$. The numerical results in Fig. 2 are consistent with earlier work on this topic in [19,42].

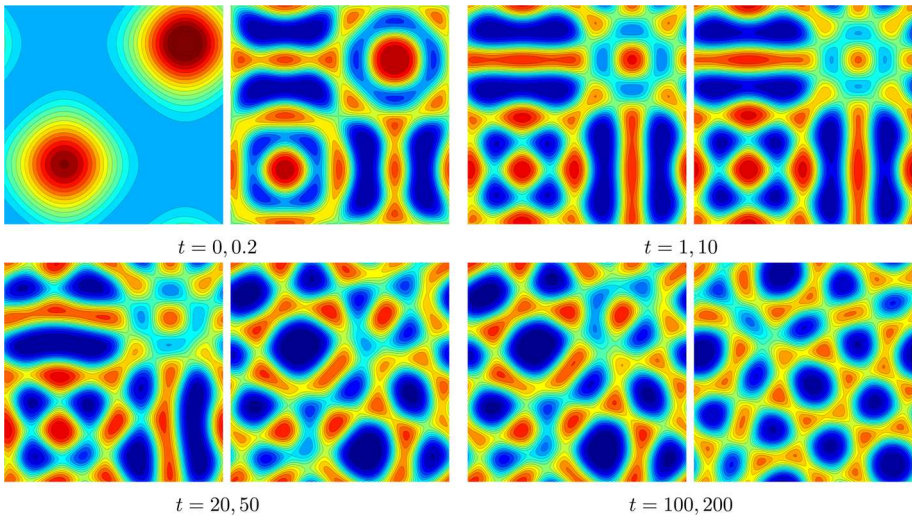

Fig. 2 Time snapshots of the benchmark problem with initial data in (6.1) at $t = 0, 0.2, 1, 10, 20, 50, 100$ and 200. The parameters are $\varepsilon = 0.18$, $\Omega = (0, 6.4)^2$, $A = 1.0$, $\eta = 1.0$, $s = 1 \times 10^{-4}$ and $h = 6.4/256$. The numerical results are consistent with earlier work on this topic in [19,42]

6.3 Spinodal Decomposition, Energy Dissipation and Mass Conservation

In the second test, we simulate the spinodal decomposition, energy-dissipation and mass-conservation. We start with the following random initial condition:

$$\phi(x, y, 0) = 0.5 + 0.05(2r - 1), \tag{6.2}$$

where r are the real random numbers in $(0, 1)$. The rest of parameters are given by $L_x = L_y = 12.8$, $\varepsilon = 0.1$, $A = 1.0$, $\eta = 1.0$, $s = 1 \times 10^{-4}$ and $h = 12.8/256$. The snapshots of spinodal decomposition with initial data in (6.2) can be found in Fig. 3. This experiment also simulates the amphiphilic di-block co-polymer mixtures of polyethylene. The numerical results are consistent with chemical experiments on this topic in [41]. Figure 4 indicates that the simulation has captured all the structural elements with hyperbolic (saddle) surfaces identified in this work, such as short cylinders with one and two beads, cylinder undulation, Y-junction and bilayer-cylinder junction can be found in zoom boxes.

The evolutions of discrete energy and mass for the simulation depicted in Fig. 3 are presented in Fig. 5. The evolution of discrete energy in Fig. 5 demonstrates the energy dissipation property, and the evolution of discrete mass clearly indicates the mass conservation property.

6.4 Meandering Instability Simulation

In addition to the micelle network, we present the simulation results of meandering instabilities [24] in this section. A temporally rescaled FCH model is used, with the following physical energy:

$$\mathcal{F}(\phi) = \frac{\gamma}{2} \int_\Omega \mu_0^2 d\mathbf{x} - \eta \mathcal{F}_0(\phi). \tag{6.3}$$

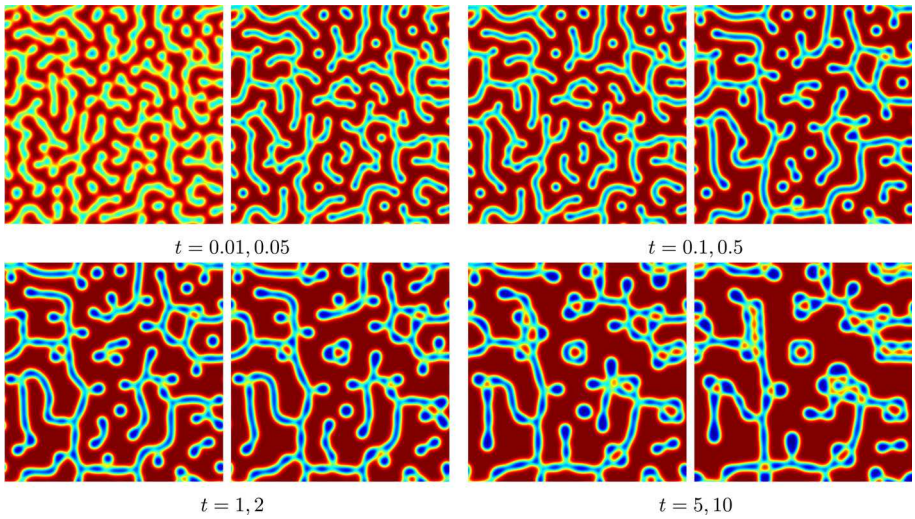

Fig. 3 Snapshots of spinodal decomposition with initial data in (6.2) at $t = 0.01, 0.05, 0.1, 0.5, 1, 2, 5$ and 10. The parameters are $\varepsilon = 0.1$, $\Omega = [0, 12.8]^2$, $A = 1.0$, $\eta = 1.0$, $s = 1 \times 10^{-4}$ and $h = 12.8/256$

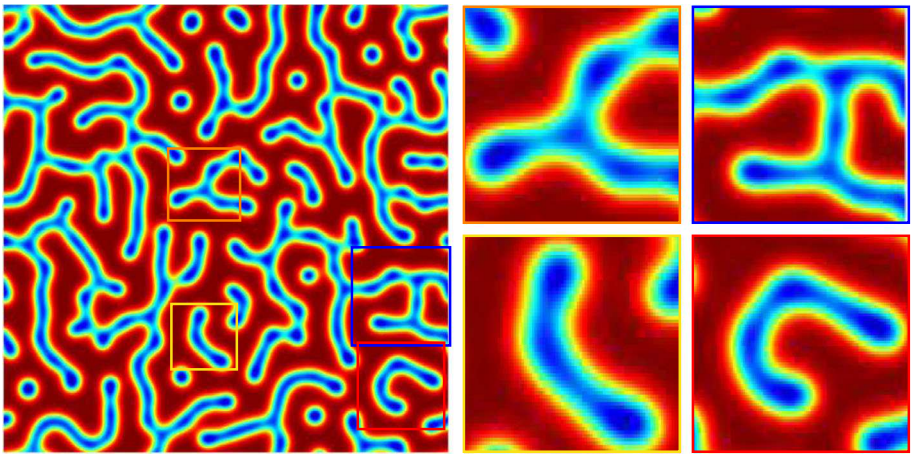

Fig. 4 Left: Snapshots of spinodal decomposition at $t = 0.05$. Right: Zoom boxes. Yellow box: Short cylinders with an undulation; Red box: Short cylinders with two undulations; Blue box: Bilayer- Cylinder junction; Orange box: Y-junction. Those numerical results are consistent with chemical experiments on this topic in [41] (Color figure online)

In turn, the convex–concave decomposition of $\mathcal{F}$ and the energy stable scheme could be derived in the same fashion as (2.15), (4.12)–(4.14).

The domain is taken as $\Omega = (0, L)^2$, with $L = 12.8$, and the following initial condition is used in the computation

$$\phi(x, y, 0) = \begin{cases} -1, & \text{if } x > \sin(\frac{4\pi y}{L}) + 6.4 + 0.34, \\ -1, & \text{if } x < \sin(\frac{4\pi y}{L}) + 6.4 - 0.34, \\ 1, & \text{otherwise.} \end{cases} \tag{6.4}$$

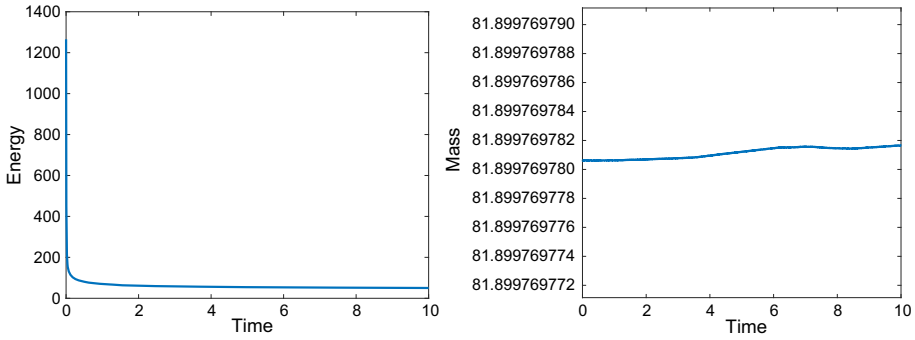

Fig. 5 The evolutions of discrete energy and mass for the simulation depicted in Fig. 3. Left: Energy Dissipation; Right: Mass Conservation

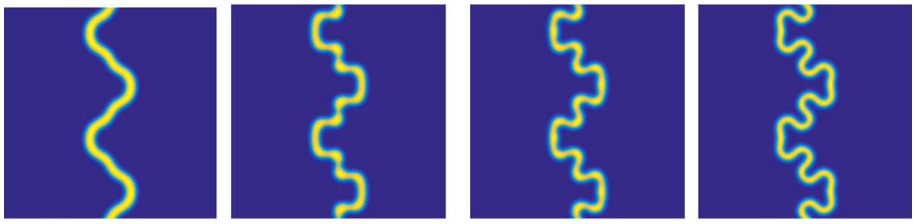

Fig. 6 Meandering instability snapshots of the phase variable with initial data (6.4) at a sequence of time instants: $t = 10$, 15, 17 and 17, over a uniform 512×512 mesh, computed by the proposed finite difference scheme (4.12)–(4.14). The parameters are $\varepsilon = 0.1$, $\Omega = [0, 12.8]^2$, $\eta = 0.2$, $s = 0.001$ and $h = 12.8/512$

The physical and numerical parameters are set as: $\varepsilon = 0.1$, $\gamma = 1$, $\eta = 0.2$, $s = 0.001$ and $h = 12.8/512$. In Fig. 6, we present the snapshot color plots of the phase variable with initial data in (6.4), computed by the convex–concave decomposition of the physical energy, in combination with the proposed second order centered difference in space. A sequence of interesting instability profiles have been observed in the numerical simulation.

To investigate the long time numerical accuracy, we also present the computational results of the second order BDF version of the first order scheme (4.12)–(4.14), namely, a numerical scheme in the form of

$$\frac{\frac{3}{2}\phi^{k+1} - 2\phi^k + \frac{1}{2}\phi^{k-1}}{s} = \Delta_h(\delta_\phi \mathcal{F}_{c,h}(\phi^{k+1}) - (2\delta_\phi \mathcal{F}_{e,h}(\phi^k) - \delta_\phi \mathcal{F}_{e,h}(\phi^{k-1})), \quad (6.5)$$

in which $\delta_\phi \mathcal{F}_{c,h}(\phi)$ and $\delta_\phi \mathcal{F}_{e,h}(\phi)$, the finite difference convex–concave decomposition profiles, have been formulated in (4.13). Of course, a theoretical justification of the energy stability for this second order accurate scheme will be much more involved, and it will be left for future works. The snapshot color plots at the same time instant sequence, produced by this second order BDF2 scheme, are displayed in Fig. 7. It is observed that these two numerical profiles are almost identical.

In addition, we also present the numerical results computed by the following Fourier pseudo-spectral scheme:

$$\frac{\phi^{k+1} - \phi^k}{s} = \Delta_N(\delta_\phi \mathcal{F}_{c,N}(\phi^{k+1}) - \delta_\phi \mathcal{F}_{e,N}(\phi^k)), \quad (6.6)$$

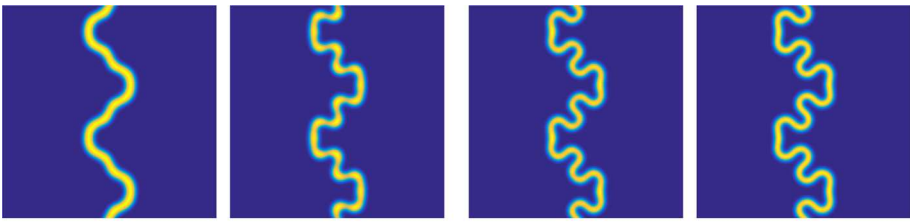

Fig. 7 Meandering instability snapshots of the numerical solution computed by the second order accurate BDF2 version of the finite difference scheme (4.12)–(4.14). The physical and numerical parameters are taken the same as Fig. 6

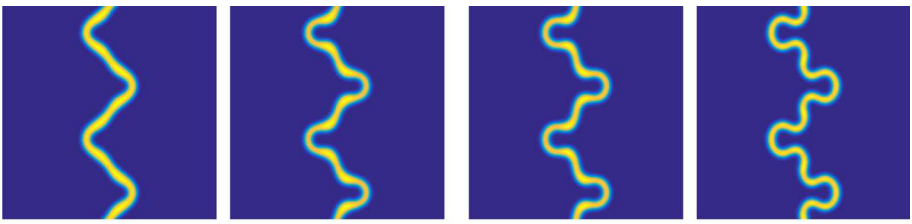

Fig. 8 Meandering instability snapshots of the numerical solution computed by the convex–concave decomposition (2.15), in combination with Fourier pseudo-spectral spatial approximation. The physical and numerical parameters are taken the same as Fig. 6

in which Δ_N stands for the Fourier pseudo-spectral approximation to the Laplacian operator, $\delta_\phi \mathcal{F}_{c,N}(\phi)$ and $\delta_\phi \mathcal{F}_{e,N}(\phi)$ are associated with the pseudo-spectral version of the convex–concave decomposition. In fact, the unique solvability, discrete energy stability and local in time convergence for the pseudo-spectral scheme could be established in a similar manner. The corresponding snapshot color plots are displayed in Fig. 8. It is observed that, the numerical profile has a similar pattern at $t = 10$, while some differences appear at later time instants $t = 15$, $t = 17$ and $t = 20$, although the general structures are still in a similar form. We notice that Fourier pseudo-spectral method yields a much smaller spatial discretization error, and a subtle difficulty associated with the staggered numerical grid has been avoided in the numerical design.

Similarly, to investigate the long time numerical accuracy of this Fourier pseudo-spectral code, we also present the numerical results computed by the second order BDF2 version; the corresponding snapshot color plots are displayed in Fig. 9. It is observed that these numerical profiles are almost identical to their version computed by the (temporally) first order scheme.

Overall, the finite difference and pseudos-spectral numerical results do not perfectly match in the long time scale. There may be a few possible reasons for such a disagreement: (1) the finite difference approximation may bring more numerical dissipations; (2) the staggered mesh used in the finite difference method, in particular for the numerical evaluation of the terms associated with the non-convex, non-concave part, $\int_\Omega 3\phi^2 |\nabla \phi|^2 \, d\mathbf{x}$, may lead to more numerical errors. In addition, the numerical differences between the Fourier pseudo-spectral and finite difference schemes may also be dependent upon the roughness of the initial data, and we notice that there is a jump discontinuity in the interface structure in (6.4). These

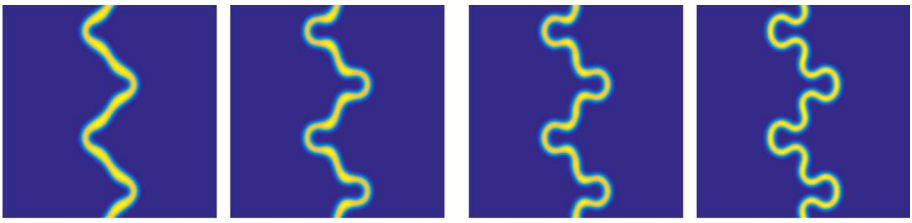

Fig. 9 Meandering instability snapshots of the numerical solution computed by the second order accurate BDF2 version of the Fourier pseudo-spectral scheme. The physical and numerical parameters are taken the same as Fig. 6

subtle issues associated with the numerical implementation will be explored in more details in the future works.

7 Conclusion

We propose and analyze an efficient numerical scheme for solving the FCH equation. Both the unique solvability and unconditional energy stability have been theoretically justified. Based on the global in time H^2_{per} stability of the numerical scheme, we present a rigorous convergence analysis. An efficient PSD method [28] is applied to solve the nonlinear system. Various numerical results are also presented, including the first order in time accuracy test, energy-dissipation, mass-conservation test, the micelle network structure and the pearling instability simulations.

Acknowledgements JSL acknowledges partial support from NSF-CHE 1035218, NSF-DMR 1105409, NSF-DMS 1217273 and DMS-FRG 1507033. CW acknowledges partial support from NSF-DMS 1418689. SMW acknowledges partial support from NSF-DMS1418692 and NSF-DMS 1719854.

References

1. Alikakos, N., Bates, P., Chen, X.: Convergence of the Cahn–Hilliard equation to the Hele–Shaw model. Arch. Ration. Mech. Anal. **128**(2), 165–205 (1994)
2. Alikakos, N., Fusco, G.: The spectrum of the Cahn–Hilliard operator for generic interface in higher space dimensions. Indiana Univ. Math. J. **42**(2), 637–674 (1993)
3. Allen, S.M., Cahn, J.W.: A microscopic theory for antiphase boundary motion and its application to antiphase domain coursening. Acta. Metall. **27**, 1085 (1979)
4. Aristotelous, A., Karakasian, O., Wise, S.: A mixed discontinuous Galerkin, convex splitting scheme for a modified Cahn–Hilliard equation and an efficient nonlinear multigrid solver. Discrete Contin. Dyn. Sys. B **18**, 2211–2238 (2013)
5. Baskaran, A., Hu, Z., Lowengrub, J., Wang, C., Wise, S., Zhou, P.: Energy stable and efficient finite-difference nonlinear multigrid schemes for the modified phase field crystal equation. J. Comput. Phys. **250**, 270–292 (2013)
6. Baskaran, A., Lowengrub, J., Wang, C., Wise, S.: Convergence analysis of a second order convex splitting scheme for the modified phase field crystal equation. SIAM J. Numer. Anal. **51**, 2851–2873 (2013)
7. Bendejacq, D., Joanicot, M., Ponsinet, V.: Pearling instabilities in water-dispersed copolymer cylinders with charged brushes. Eur. Phys. J. E **17**, 83–92 (2005)
8. Boyd, J.P.: Chebyshev and Fourier Spectral Methods. Courier Corporation, North Chelmsford (2001)
9. Cahn, J.: On spinodal decomposition. Acta Metall. **9**, 795 (1961)

10. Cahn, J., Hilliard, J.: Free energy of a nonuniform system. I. interfacial free energy. J. Chem. Phys. **28**, 258 (1958)
11. Chen, F., Shen, J.: Efficient spectral-Galerkin methods for systems of coupled second-order equations and their applications. J. Comput. Phys. **231**, 5016–5028 (2012)
12. Chen, W., Conde, S., Wang, C., Wang, X., Wise, S.: A linear energy stable scheme for a thin film model without slope selection. J. Sci. Comput. **52**, 546–562 (2012)
13. Chen, W., Liu, Y., Wang, C., Wise, S.: An optimal-rate convergence analysis of a fully discrete finite difference scheme for Cahn–Hilliard–Hele–Shaw equation. Math. Comput. **85**, 2231–2257 (2016)
14. Chen, W., Wang, C., Wang, X., Wise, S.: A linear iteration algorithm for energy stable second order scheme for a thin film model without slope selection. J. Sci. Comput. **59**, 574–601 (2014)
15. Chen, X.: Spectrum for the Allen–Cahn Cahn–Hilliard and phase-field equations for generic interfaces. Commun. Partial Differ. Equ. **19**, 1371–1395 (1994)
16. Chen, X.: Global asymptotic limit of solutions of the Cahn–Hilliard equation. J. Differ. Geom. **44**(2), 262–311 (1996)
17. Chen, X., Elliott, C.M., Gardiner, A., Zhao, J.: Convergence of numerical solutions to the Allen–Cahn equation. Appl. Anal. **69**(1), 47–56 (1998)
18. Cheng, K., Feng, W., Gottlieb, S., Wang, C.: A Fourier pseudospectral method for the "Good" Boussinesq equation with second-order temporal accuracy. Numer. Methods Partial Differ. Equ. **31**, 202–224 (2015)
19. Christlieb, A., Jones, J., Promislow, K., Wetton, B., Willoughby, M.: High accuracy solutions to energy gradient flows from material science models. J. Comput. Phys. **257**, 193 Part A–215 (2014)
20. Dai, S., Promislow, K.: Geometric evolution of bilayers under the Functionalized Cahn–Hilliard equation. In: Proceedings of the Royal Society of London A: Mathematical, Physical and Engineering Sciences, p 469 (2013)
21. Diegel, A., Feng, X., Wise, S.: Analysis of a mixed finite element method for a Cahn–Hilliard–Darcy–Stokes system. SIAM J. Numer. Anal. **53**, 127–152 (2015)
22. Diegel, A., Wang, C., Wang, X., Wise, S.: Convergence analysis and error estimates for a second order accurate finite element method for the Cahn–Hilliard–Navier–Stokes system. Numer. Math. **137**, 495–534 (2017)
23. Diegel, A., Wang, C., Wise, S.: Stability and convergence of a second order mixed finite element method for the Cahn–Hilliard equation. IMA J. Numer. Anal. **36**, 1867–1897 (2016)
24. Doelman, A., Hayrapetyan, G., Promislow, K., Wetton, B.: Meander and pearling of single-curvature bilayer interfaces in the Functionalized Cahn–Hilliard equation. SIAM J. Math. Anal. **46**, 3640–3677 (2014)
25. Dong, L., Feng, W., Wang, C., Wise, S., Zhang, Z.: Convergence analysis and numerical implementation of a second order numerical scheme for the three-dimensional phase field crystal equation. Comput. Math. Appl. (2018). https://doi.org/10.1016/j.camwa.2017.07.012
26. Eyre, D.: Unconditionally gradient stable time marching the Cahn–Hilliard equation. In: Bullard, J.W., Kalia, R., Stoneham, M., Chen, L. (eds.) Computational and Mathematical Models of Microstructural Evolution, vol. 53, pp. 1686–1712. Materials Research Society, Warrendale (1998)
27. Feng, W., Guo, Z., Lowengrub, J., Wise, S.: A mass-conservative adaptive FAS multigrid solver for cell-centered finite difference methods on block-structured, locally-cartesian grids. J. Comput. Phys. **352**, 463–497 (2018)
28. Feng, W., Salgado, A., Wang, C., Wise, S.: Preconditioned steepest descent methods for some nonlinear elliptic equations involving p-Laplacian terms. J. Comput. Phys. **334**, 45–67 (2017)
29. Feng, W., Wang, C., Wise, S., Zhang, Z.: A second-order energy stable Backward Differentiation Formula method for the epitaxial thin film equation with slope selection. Numer. Methods Partial Differ. Equ. (Submitted and in review, 2018)
30. Feng, X., Li, Y.: Analysis of interior penalty discontinuous Galerkin methods for the Allen–Cahn equation and the mean curvature flow. IMA J. Numer. Anal. **35**, 1622–1651 (2015)
31. Feng, X., Li, Y., Xing, Y.: Analysis of mixed interior penalty discontinuous Galerkin methods for the Cahn–Hilliard equation and the Hele–Shaw flow. SIAM J. Numer. Anal. **54**, 825–847 (2016)
32. Feng, X., Prohl, A.: Error analysis of a mixed finite element method for the Cahn–Hilliard equation. Numer. Math. **99**, 47–84 (2004)
33. Gavish, N., Hayrapetyan, G., Promislow, K., Yang, L.: Curvature driven flow of bi-layer interfaces. Phys. D Nonlinear Phenom. **240**, 675–693 (2011)
34. Gavish, N., Jones, J., Xu, Z., Christlieb, A., Promislow, K.: Variational models of network formation and ion transport: applications to perfluorosulfonate ionomer membranes. Polymers **4**, 630–655 (2012)
35. Gompper, G., Schick, M.: Correlation between structural and interfacial properties of amphiphilic systems. Phys. Rev. Lett. **65**, 1116–1119 (1990)

36. Guo, J., Wang, C., Wise, S., Yue, X.: An H^2 convergence of a second-order convex-splitting, finite difference scheme for the three-dimensional Cahn–Hilliard equation. Commu. Math. Sci. **14**, 489–515 (2016)
37. Guo, R., Xu, Y., Xu, Z.: Local discontinuous Galerkin methods for the functionalized Cahn–Hilliard equation. J. Sci. Comput. **63**, 913–937 (2015)
38. Hesthaven, J.S., Gottlieb, S., Gottlieb, D.: Spectral Methods for Time-Dependent Problems, vol. 21. Cambridge University Press, Cambridge (2007)
39. Hsu, W.Y., Gierke, T.D.: Ion transport and clustering in nafion perfluorinated membranes. J. Membr. Sci. **13**, 307–326 (1983)
40. Hu, Z., Wise, S., Wang, C., Lowengrub, J.: Stable and efficient finite-difference nonlinear-multigrid schemes for the phase field crystal equation. J. Comput. Phys. **228**, 5323–5339 (2009)
41. Jain, S., Bates, F.S.: Consequences of nonergodicity in aqueous binary PEO-PB micellar dispersions. Macromolecules **37**, 1511–1523 (2004)
42. Jones, J.: Development of a fast and accurate time stepping scheme for the Functionalized Cahn–Hilliard equation and application to a graphics processing unit. Ph.D. thesis, Michigan State University (2013)
43. Li, W., Chen, W., Wang, C., Yan, Y., He, R.: A second order energy stable linear scheme for a thin film model without slope selection. J. Sci. Comput. (in press, 2018)
44. Promislow, K., Wetton, B.: Pem fuel cells: a mathematical overview. SIAM J. Appl. Math. **70**, 369–409 (2009)
45. Promislow, K., Wu, Q.: Existence of pearled patterns in the planar functionalized Cahn–Hilliard equation. J. Differ. Equ. **259**, 3298–3343 (2015)
46. Shen, J., Wang, C., Wang, X., Wise, S.: Second-order convex splitting schemes for gradient flows with Ehrlich-Schwoebel type energy: application to thin film epitaxy. SIAM J. Numer. Anal. **50**, 105–125 (2012)
47. Torabi, S., Lowengrub, J., Voigt, A., Wise, S.: A new phase-field model for strongly anisotropic systems. In: Proceedings of the Royal Society of London A, The Royal Society, pp. rspa–2008 (2009)
48. Torabi, S., Wise, S., Lowengrub, J., Ratz, A., Voigt, A.: A new method for simulating strongly anisotropic Cahn–Hilliard equations. In: MST 2007 Conference Proceedings, vol. 3, p. 1432 (2007)
49. Wang, C., Wang, X., Wise, S.: Unconditionally stable schemes for equations of thin film epitaxy. Discrete Contin. Dyn. Syst. A **28**, 405–423 (2010)
50. Wang, C., Wise, S.M.: An energy stable and convergent finite-difference scheme for the modified phase field crystal equation. SIAM J. Numer. Anal. **49**, 945–969 (2011)
51. Wang, X., Ju, L., Du, Q.: Efficient and stable exponential time differencing Runge-Kutta methods for phase field elastic bending energy models. J. Comput. Phys. **316**, 21–38 (2016)
52. Wise, S., Kim, J., Lowengrub, J.: Solving the regularized, strongly anisotropic Cahn–Hilliard equation by an adaptive nonlinear multigrid method. J. Comput. Phys. **226**, 414–446 (2007)
53. Wise, S., Wang, C., Lowengrub, J.: An energy stable and convergent finite-difference scheme for the phase field crystal equation. SIAM J. Numer. Anal. **47**, 2269–2288 (2009)
54. Yan, Y., Chen, W., Wang, C., Wise, S.: A second-order energy stable BDF numerical scheme for the Cahn–Hilliard equation. Commun. Comput. Phys. **23**, 572–602 (2018)